Molecular Biology of the Cell
Vol. 21, 2930–2943, August 15, 2010

EHBP-1 Functions with RAB-10 during Endocytic Recycling in *Caenorhabditis elegans*

Anbing Shi,*† Carlos Chih-Hsiung Chen,*†‡ Riju Banerjee,* Doreen Glodowski,‡ Anjon Audhya,§ Christopher Rongo,‡ and Barth D. Grant*

*Department of Molecular Biology and Biochemistry, ‡Department of Genetics and the Waksman Institute, Rutgers University, Piscataway, NJ 08854; and §Department of Biomolecular Chemistry, University of Wisconsin-Madison, Madison, WI 53706

Submitted February 22, 2010; Revised June 4, 2010; Accepted June 10, 2010
Monitoring Editor: Francis A. Barr

Caenorhabditis elegans **RAB-10 functions in endocytic recycling in polarized cells, regulating basolateral cargo transport in the intestinal epithelia and postsynaptic cargo transport in interneurons. A similar role was found for mammalian Rab10 in MDCK cells, suggesting that a conserved mechanism regulates these related pathways in metazoans. In a yeast two-hybrid screen for binding partners of RAB-10 we identified EHBP-1, a calponin homology domain (CH) protein, whose mammalian homolog Ehbp1 was previously shown to function during endocytic transport of GLUT4 in adipocytes. In vivo we find that EHBP-1-GFP colocalizes with RFP-RAB-10 on endosomal structures of the intestine and interneurons and that *ehbp-1* loss-of-function mutants share with *rab-10* mutants specific endosome morphology and cargo localization defects. We also show that loss of EHBP-1 disrupts transport of membrane proteins to the plasma membrane of the nonpolarized germline cells, a defect that can be phenocopied by codepletion of RAB-10 and its closest paralog RAB-8. These results indicate that RAB-10 and EHBP-1 function together in many cell types and suggests that there are differences in the level of redundancy among Rab family members in polarized versus nonpolarized cells.**

INTRODUCTION

The endocytic pathways of eukaryotes regulate the uptake, sorting, and the subsequent recycling or degradation of macromolecules, fluid, membranes, and membrane proteins. After endocytosis through either clathrin-dependent or one of several clathrin-independent uptake mechanisms (Nichols, 2003; Gesbert *et al.,* 2004), cargo proteins are delivered to early endosomes, where sorting occurs. Some cargo will be sorted for delivery to lysosomes for degradation (Mukherjee *et al.,* 1997), whereas others will be directly or indirectly routed back to the plasma membrane or Golgi apparatus through various recycling pathways (Maxfield and McGraw, 2004; Rojas *et al.,* 2007; Grant and Donaldson, 2009).

The Rab family of GTPases function as master regulators, controlling diverse aspects of intracellular trafficking and organelle identity (Stenmark, 2009). Like other Ras superfamily GTPases, Rabs cycle between an active GTP-bound state and an inactive GDP-bound state. Through their direct or indirect interactions with effectors and binding proteins, Rabs function as coordinators of intracellular trafficking events, often controlling motor-based delivery of vesicles and vesicle tethering, and in some cases affecting cargo recruitment, vesicle budding, and vesicle fusion with target compartment membranes (Grosshans *et al.,* 2006; Stenmark, 2009).

Rabs have been shown to regulate both fast recycling directly from early endosomes and slow recycling from the endocytic recycling compartment (ERC; Grant and Donaldson, 2009). Rab4 was identified as an important regulator of transferrin receptor (TfR) recycling (van der Sluijs *et al.,* 1992), although the precise function of Rab4 in recycling remains unclear. Studies by Kouranti *et al.* (2006) indicated that Rab35 is also an important regulator of TfR rapid recycling, whereas other studies indicate a role for Rab35 on the Arf6- and EHD1-containing tubular endosomes of the slow recycling pathway (Walseng *et al.,* 2008; Allaire *et al.,* 2010). Another well-established Rab involved in recycling is Rab11, a resident of the ERC that mediates recycling from the ERC to the plasma membrane (Powelka *et al.,* 2004; Weigert *et al.,* 2004). In polarized cells, Rab11 activity appears restricted to the apical membrane, whereas other proteins must regulate recycling to the basolateral surface. Thus, polarized cells appear to use different mechanisms to regulate trafficking at their distinct, specialized membrane surfaces.

Regulated recycling has also been demonstrated in nonpolarized cells. Interestingly, such cells still employ multiple mechanisms in the trafficking of different recycling cargo. For instance in HeLa cells Arf6 and Rab22a are important for the recycling of major histocompatibility complex (MHC) class I and TAC (IL2-receptor α chain), but have little or no effect on TfR (Weigert *et al.,* 2004). MHCI and TAC are internalized by clathrin-independent endocytosis (CIE), whereas TfR is internalized by clathrin-dependent endocytosis (CDE). The two cargo classes appear to converge in the endosomal system after uptake, but diverge again upon exit from the ERC. It remains unclear if their divergence in recycling is related to the difference in their uptake routes.

This article was published online ahead of print in *MBoC in Press* (http://www.molbiolcell.org/cgi/doi/10.1091/mbc.E10–02–0149) on June 23, 2010.

†These authors contributed equally to this work.

Address correspondence to: Barth D. Grant (grant@biology.rutgers.edu).

© 2010 by The American Society for Cell Biology

Rab11 and EHD1 proteins are important for the recycling of both cargo types, although there are likely to be differences in the mechanisms used to recycle these two cargo types.

RAB-10 has been implicated in the recycling of clathrin-independent cargo in the *Caenorhabditis elegans* intestine, probably at the level of transport between early endosomes and recycling endosomes (Chen *et al.*, 2006). Recent work in *C. elegans* suggests that interneuron postsynaptic glutamate receptor recycling also requires RAB-10 (Glodowski *et al.*, 2007). In mammalian systems, Rab10 has been implicated in basolateral recycling in Madin-Darby canine kidney (MDCK) cells and in Glut4 recycling in adipocytes (Babbey *et al.*, 2006; Sano *et al.*, 2007). RAB-10, and another similar GTPase, RAB-8, are the closest metazoan relatives of yeast Sec4p, the final Rab in the yeast secretory pathway. Rab8 has been suggested to function in the secretory pathway in mammalian cells (Hattula *et al.*, 2002; Ang *et al.*, 2003), and this delivery process may use the recycling endosomes as an intermediate (Ang *et al.*, 2004; Henry and Sheff, 2008). In polarized MDCK cells, simultaneous knockdown of Rab8 and Rab10 produced more severe exocytosis defects than individual knockdown (Schuck *et al.*, 2007), implying that Rab8 and Rab10 may function redundantly in exocytic membrane trafficking, perhaps by sharing some effectors. Whether the different Rabs that regulate distinct recycling pathways use different effector molecules remains an open question.

Here we report the physical association of RAB-10 and -8 with the effector molecule EHBP-1. We show that *ehbp-1* mutants share several specific recycling defects with *rab-10* mutants, including preferential effects on the CIE cargo protein TAC in the intestine. We also provide evidence that EHBP-1 functions with RAB-10 in neurons and regulates germ cell growth in a pathway that is redundantly regulated by RAB-10 and -8. Surprisingly, unlike conventional Rab effectors, our results suggest that EHBP-1 functions upstream of RAB-10 and is important for the endosomal association of RAB-10.

MATERIALS AND METHODS

General Methods and Strains

All *C. elegans* strains were derived originally from the wild-type Bristol strain N2. Worm cultures, genetic crosses, and other *C. elegans* husbandry were performed according to standard protocols (Brenner, 1974). Strains expressing transgenes were grown at 20°C. A complete list of strains used in this study can be found in Supplementary Table 1.

RNA interference (RNAi) was performed using the feeding method (Timmons and Fire, 1998). Feeding constructs were either from the Ahringer library (Kamath and Ahringer, 2003) or were prepared by PCR from EST clones provided by Dr. Yuji Kohara (National Institute of Genetics, Japan) followed by subcloning into the RNAi vector L4440 (Timmons and Fire, 1998). For most experiments synchronized L1 or L4 stage animals were treated for 24–72 h and were scored as adults.

Antibodies

The following antibodies were used in this study: mouse anti-HA mAb (16B12; Covance Research Products, Berkeley, CA), rabbit anti-GST polyclonal antibody (Z-5; Santa Cruz Biotechnology. Santa Cruz, CA).

Yeast Two-Hybrid Analyses

Yeast two-hybrid screen for candidates of RAB-10–interacting proteins was performed according to the procedure of the DupLEX-A yeast two-hybrid system (OriGene Technologies, Rockville, MD). The cDNA sequences of *C. elegans rab-10(Q68L)* in the entry vector pDONR221 were cloned into the pEG202-Gtwy bait vector by Gateway recombination cloning (Invitrogen, Carlsbad, CA) to generate N-terminal fusions with the LexA DNA-binding domain. The pEG202-rab-5(Q78L), rab-7(Q68L), rab-8(Q67L), rab-11(Q70L), rab-35(Q69L), rme-1 and inactive rab-10(QT23N), and rab-8(QT23N) were constructed accordingly. The prenylation motifs for membrane attachment at the C-terminal ends of each RAB were also deleted to improve entry of bait fusion proteins into the yeast nucleus. The *C. elegans* cDNA library was purchased from the DupLEX-A yeast two-hybrid system (OriGene Technologies, Rockville, MD).

All two-hybrid plasmids were generated as PCR products with Gateway attB.1 and attB.2 sequence extensions and were introduced into the Gateway entry vector pDONR221 by BP reaction. The bait vector pEG202-Gtwy and target vector pJG4–5-Gtwy have been described previously (Sato *et al.*, 2008b). Prey plasmids encoded EHBP-1 truncations were amplified from *C. elegans* EST clone *yk1543d03* (Dr. Yuji Kohara), and all amplified regions were confirmed by DNA sequencing. OriGene plasmid pSH18–34 [*URA3*, 8 ops.-LacZ] was used as reporter in all the yeast two-hybrid experiments. Constructs were introduced into the yeast strain EGY48 [MATα trp1 his3 ura3 leu2::6 LexAop-*LEU2*] included in the system. Transformants were selected on plates lacking leucine, histidine, tryptophan, and uracil, containing 2% galactose/1% raffinose at 30°C for 3 d and assayed for the expression of the *LEU2* reporter. Blue/white β-galactosidase assays confirmed results shown for growth assays, according to manufacturer's instructions.

Tissue-specific Steady-State Endocytosis Assays

Intestinal basolateral endocytosis was visualized using muscle-secreted green fluorescent protein (GFP; transgenic strain *arIs37[myo-3::ssGFP]*) as a fluid-phase marker in a *cup-4* mutant background. The *cup-4* mutation was included to reduce uptake by coelomocytes and increase availability of the marker in the body cavity (Patton *et al.*, 2005).

Protein Expression and Coprecipitation Assays

N-terminally hemagglutinin (HA)-tagged proteins, RAB-5(Q78L), RAB-7(Q68L), RAB-8(Q67L), and RAB-10(Q68L), were synthesized in vitro using the TNT-coupled transcription-translation system (Promega, Madison, WI) using DNA templates pcDNA3.1–2xHA-RAB-5(Q78L), pcDNA3.1–2xHA-RAB-7(Q68L), pcDNA3.1–2xHA-RAB-8(Q67L), and pcDNA3.1–2xHA-RAB-10(Q68L), respectively (1.6 μg/each 50-μl reaction). The reaction cocktail was incubated at 30°C for 90 min. Control glutathione *S*-transferase (GST) and GST-EHBP-1(aa 662–901) fusion proteins were expressed in the *ArcticExpress* strain of *Escherichia coli* (Stratagene, La Jolla, CA). Bacterial pellets were lysed in 10 ml B-PER Bacterial Protein Extraction Reagent (Pierce, Rockford, ILL) with Complete Protease Inhibitor Cocktail Tablets (Roche, Indianapolis, IN). Extracts were cleared by centrifugation, and supernatants were incubated with glutathione-Sepharose 4B beads (Amersham Pharmacia, Piscataway, NJ) at 4°C overnight. Beads were then washed six times with cold STET buffer (10 mM Tris-HCl, pH 8.0, 150 mM NaCl, 1 mM EDTA, 0.1% Tween-20). In vitro–synthesized HA-tagged protein (10 μl TNT mix diluted in 500 μl STET) was added to the beads and allowed to bind at 4°C for 2 h. After six additional washes in STET the proteins were eluted by boiling in 30 μl 2× SDS-PAGE sample buffer. Eluted proteins were separated on SDS-PAGE (10% polyacrylamide), blotted to nitrocellulose, and probed with anti-HA (16B12). Subsequently the blots were stripped and reprobed with anti-GST (Z-5) antibodies.

Plasmids and Transgenic Strains

rab-5(Q78L), *rab-7*(Q68L), *rab-8*(Q67L), and *rab-10*(Q68L) cDNA clones were transferred into an in-house modified vector pcDNA3.1 (+) (Invitrogen) with 2xHA epitope tag and Gateway cassette (Invitrogen) for in vitro transcription/translation experiments. For GST pulldown experiments an equivalent *ehbp-1*(aa 662–901) PCR product was introduced in frame into vector pGEX-2T (GE Healthcare Life Sciences, Piscataway, NJ) modified with a Gateway cassette.

To construct the GFP-tagged *ehbp-1* transgene driven by its own promoter, *ehbp-1* genomic sequences and presumed promoter sequences were PCR amplified from *C. elegans* genomic DNA, cloned into the entry vector pDONR221, and then transferred into the *C. elegans* pPD117.01 vector with Gateway cassettes (Invitrogen) followed by GFP coding sequences, *let-858* 3′ UTR sequences and the *unc-119* gene of *C. briggsae*. The GFP-tagged plasmids (10 μg each) were bombarded into *unc-119(ed3)* mutant animals to establish low copy integrated transgenic lines by microparticle bombardment method (Praitis *et al.*, 2001). Integrated transgenic lines used in this study are listed in Supplementary Table 1.

To construct GFP or RFP/mCherry (a gift from R. Tsien, University of California, San Diego) fusion transgenes for expression specifically in the worm intestine, a previously described *vha-6* promoter-driven vector modified with a Gateway cassette inserted at the Asp718I site just upstream of the GFP or red fluorescent protein (RFP) coding region was used. The sequences of *C. elegans ehbp-1(cDNA)* and *ehbp-1(aa1–711)* lacking a stop codon were cloned individually into entry vector pDONR221 by PCR and BP reaction, and then transferred into intestinal expression vectors by Gateway recombination cloning LR reaction to generate C-terminal fusions (Chen *et al.*, 2006). Complete plasmid sequences are available on request. Low copy integrated transgenic lines for all of these plasmids were obtained by the microparticle bombardment method (Praitis *et al.*, 2001).

Transgenic strains used in the GLR-1 glutamate receptor trafficking study were isolated after microinjecting various plasmids (5–50 ng/μl) along with *rol-6dm* (a gift from C. Mello, University of Massachusetts Medical School) or ttx-3::rfp as a transgenic marker (monomeric RFP; a gift from R. Tsien). Plasmids containing the *glr-1* promoter, followed by a gene encoding either

RFP::RAB-10 or EHBP-1::GFP, were introduced into the germline by microinjection or microparticle bombardment, and followed as extrachromosomal arrays. To generate these plasmids, LR reactions (Gateway Technology; Invitrogen) were performed using entry clones containing genomic DNA encoding EHBP-1 or cDNA encoding RAB-10. For these reactions, the destination vector, which contains the *glr-1* promoter upstream of a *ccdB* gene that is flanked by *attR* sites, was generated from the plasmid pV6 (a gift from V. Maricq, University of Utah), following manufacturer's protocols (Invitrogen). For RFP-RAB-10, stable transgenic lines, including *odIs42*, were obtained by γ-irradiation followed by four generations of backcrossing.

Microscopy and Image Analysis

Live worms were mounted on 2% agarose pads with 10 mM levamisol as described previously (Sato *et al.*, 2005). Multiwavelength fluorescence images were obtained using an Axiovert 200M (Carl Zeiss MicroImaging, Oberkochen, Germany) microscope equipped with a digital CCD camera (C4742–12ER, Hamamatsu Photonics, Hamamatsu, Japan), captured using Metamorph software ver. 6.3r2 (Universal Imaging, West Chester, PA) and then deconvolved using AutoDeblur Gold software ver. 9.3 (AutoQuant Imaging, Watervliet, NY). Images taken in the DAPI channel were used to identify broad-spectrum intestinal autofluorescence caused by lipofuscin-positive lysosome-like organelles (Clokey and Jacobson, 1986; Hermann *et al.*, 2005). To obtain images of GFP fluorescence without interference from autofluorescence, we used argon 488-nm excitation and the spectral fingerprinting function of the Zeiss LSM510 Meta confocal microscope system (Carl Zeiss MicroImaging) as described previously (Chen *et al.*, 2006). Quantification of images was performed with Metamorph software ver. 6.3r2 (Universal Imaging). Most GFP/RFP colocalization experiments were performed on L3 and L4 larvae expressing GFP and RFP markers as previously described.

For fluorescence microscopy of *C. elegans* ventral cord neurites, details were as described previously, but with some modifications (Glodowski *et al.*, 2007). GFP- and RFP-tagged fluorescent proteins were visualized in nematodes by mounting young adults (16–18 h post-L4 stage) on 2% agarose pads with 100 mM tetramisole in M9 buffer. Fluorescent images were obtained using an Axioplan II (Carl Zeiss, Thornwood, NY). A 100× (NA 1.4) PlanApo objective was used to detect GFP and RFP signals. Imaging was done with an ORCA charge-coupled device camera (Hamamatsu, Bridgewater, NJ) by using iVision software (Scanalytics, Fairfax, VA). Exposure times were chosen to fill the 12-bit dynamic range without saturation. Maximum intensity projections of z-series stacks were obtained, and out-of-focus light was removed with a constrained iterative deconvolution algorithm. Puncta outlines were automatically calculated for fluorescent signals that were two SDs above the unlocalized baseline by using a macro written for ImageJ64 software (http://rsb.info.nih.gov/ij/). Puncta size was measured as the maximum diameter for each outlined cluster. Puncta outline data included both small puncta (e.g., as observed GLR-1-GFP and GFP-RAB-10 in wild type, classified based on a diameter cutoff of <1 μm and circular morphology using a program written in ImageJ), as well as long accretions (e.g., as observed GFP-RAB-10 in wild-type and GLR-1-GFP in *rab-10* and *ehbp-1* mutants, classified based on a width cutoff of >1 μm and elongated morphology). Numbers were calculated by counting the average number of small puncta or large accretions per 10 or 100 μm of neurite length, respectively.

Behavioral Assays

The reversal frequency of individual animals was assayed as described previously, but with some modifications (Zheng *et al.*, 1999). Single young adult hermaphrodites were placed on nematode growth medium plates in the absence of food. The animals were allowed to adjust to the plates for 5 min, and the number of spontaneous reversals for each animal was counted over a 5-min period. Thirty animals were tested for each genotype, and the reported scores reflect the mean number of reversals per minute.

Protein Secretion Assay in the C. elegans Germline

The generation of a *C. elegans* strain expressing mCherry-PH $^{PLC1\delta1}$ has been described previously (Kachur *et al.*, 2008). A GFP fusion to SNB-1 (T10H9.4) was generated by cloning the unspliced genomic locus into the SpeI site of pIC26 (GFP; Cheeseman *et al.*, 2004). The construct was integrated into DP38 *[unc-119 (ed3)]* as described previously (Praitis *et al.*, 2001) using a particle delivery system (Biolistic PDS-1000/He; Bio-Rad Laboratories, Richmond, CA).

Double-stranded RNA (dsRNA) was prepared as described previously (Oegema *et al.*, 2001) from templates prepared by using the primers listed (below) to amplify N2 genomic DNA. For depletions, L4 hermaphrodites were injected with dsRNA and incubated at 20°C for 45 h before analysis. The following primers were used: RNA 210, D1037.4, RAB-8, 1.9 mg/ml: oligo 1: AATTAACCCTCACTAAAGGgcttttgcatgccaagatgtc and oligo 2: TAATACGACTCACTATAGGCGGGACGAAAATGGTAAAAA; RNA 311, T23H2.5, RAB-10, 2.3 mg/ml: oligo 1: AATTAACCCTCACTAAAGGGTGCTGCTAATAGGCGACTCA and oligo 2: TAATACGACTCACTATAGGTTGCTCGTCAGTGGAATCAG; and RNA KOEHBP-1, F25B3.1, EHBP-1, 2.4 mg/ml: oligo 1: AATTAACCCTCACTAAAGGGATTTCAGTTCGTCCCCAATG and oligo 2: TAATACGACTCACTATAGGACGAATTGCTCCAACTCCTG.

For analysis of gonads, animals were anesthetized in 0.1% tricane (Sigma, St. Louis, MO), mounted on agarose pads and imaged at 20°C on a spinning disk confocal (Eclipse TE2000-E; Nikon, Melville, NY) microscope equipped with a Nikon 60×, 1.4NA PlanApo oil objective lens and a Hamamatsu ORCA-ER CCD camera. Line-scan analysis was performed using Metamorph software (Universal Imaging).

RESULTS

EHBP-1 Associates with Active GTP-bound RAB-10

To identify other proteins that function with RAB-10 in endocytic recycling, we performed a yeast two-hybrid screen for binding partners of the active GTP-bound form of RAB-10, using a predicted constitutively active mutant, RAB-10(Q68L), as bait. We identified 27 positive interacting clones encoding C-terminal portions of EHBP-1, the only *C. elegans* homolog of mammalian Ehbp1, a protein previously implicated in Glut4 trafficking in mammalian adipocytes (Guilherme *et al.*, 2004b). Previous reports on mammalian Ehbp1 had not linked it to a Rab GTPase, but rather to EHD1 and EHD2, two membrane-associated proteins of the RME-1 ATPase family, which function in membrane tubulation and potentially in membrane fission (Guilherme *et al.*, 2004b; Pant *et al.*, 2009). The smallest recovered interacting clone encompassed EHBP-1 amino acids 662–901 (Figure 1A and *Materials and Methods*). We further delimited the RAB-10–interacting domain of EHBP-1 to amino acids 712–851, a predicted coiled-coil region of the protein (Figure 1, C and D). No interaction could be detected between the C-terminal region of EHBP-1 and RAB-10(T23N), a predicted constitutively inactive GDP-bound mutant form of the Rab (Figure 1B and Supplemental Figure S1, A and B). These data suggest that EHBP-1 specifically binds to the active GTP-bound form of RAB-10.

We next screened other Rab GTPases for their ability to bind EHBP-1 using the yeast two-hybrid system. We found that GTP-bound RAB-8(Q67L), but not GDP-bound RAB-8(T23N), also bound to EHBP-1, including the minimal binding domain of EHBP-1(aa 712–851) defined by interaction with RAB-10 (Figure 1B and Supplemental Figure S2). RAB-8 is the closest paralog of RAB-10 in *C. elegans*, and together RAB-8 and -10 represent a branch of the metazoan Rabs that in vertebrates also includes Rab13, which is not present in the worm (Pereira-Leal and Seabra, 2001). We did not detect interactions between EHBP-1 and the active forms of several other Rabs, including RAB-5, -7, -11, or -35 (Figure 1B). We further confirmed the binding interaction between RAB-8/10 with EHBP-1 using an in vitro GST-pulldown assay (Figure 1A and *Materials and Methods*). Surprisingly, this assay also detected a weak interaction with RAB-5(Q78L) that could not be detected using the two-hybrid method (Figure 1A). Together, these data indicate that EHBP-1 is a Rab-interacting protein, with a strong preference for the active forms of RAB-8 and -10.

In previous studies, we showed that RME-1, a regulator of endocytic recycling, functions downstream of RAB-10 (Chen *et al.*, 2006). Two mammalian homologues of RME-1, called EHD1 and EHD2, have been shown to interact with Ehbp1 in a manner dependent on the five closely spaced NPF motifs within Ehbp1 (Guilherme *et al.*, 2004a,b). However, *C. elegans* EHBP-1 lacks NPF motifs, and we were unable to detect any interaction between the *C. elegans* proteins RME-1 and EHBP-1 using the yeast two-hybrid system, suggesting that this interaction is not conserved (Figure 1B and Supplemental Figure S1, C and D). Indeed, sequence alignment of Ehbp1/EHBP-1 orthologues shows that the NPF motifs are well conserved among vertebrate Ehbp1 homologues, but

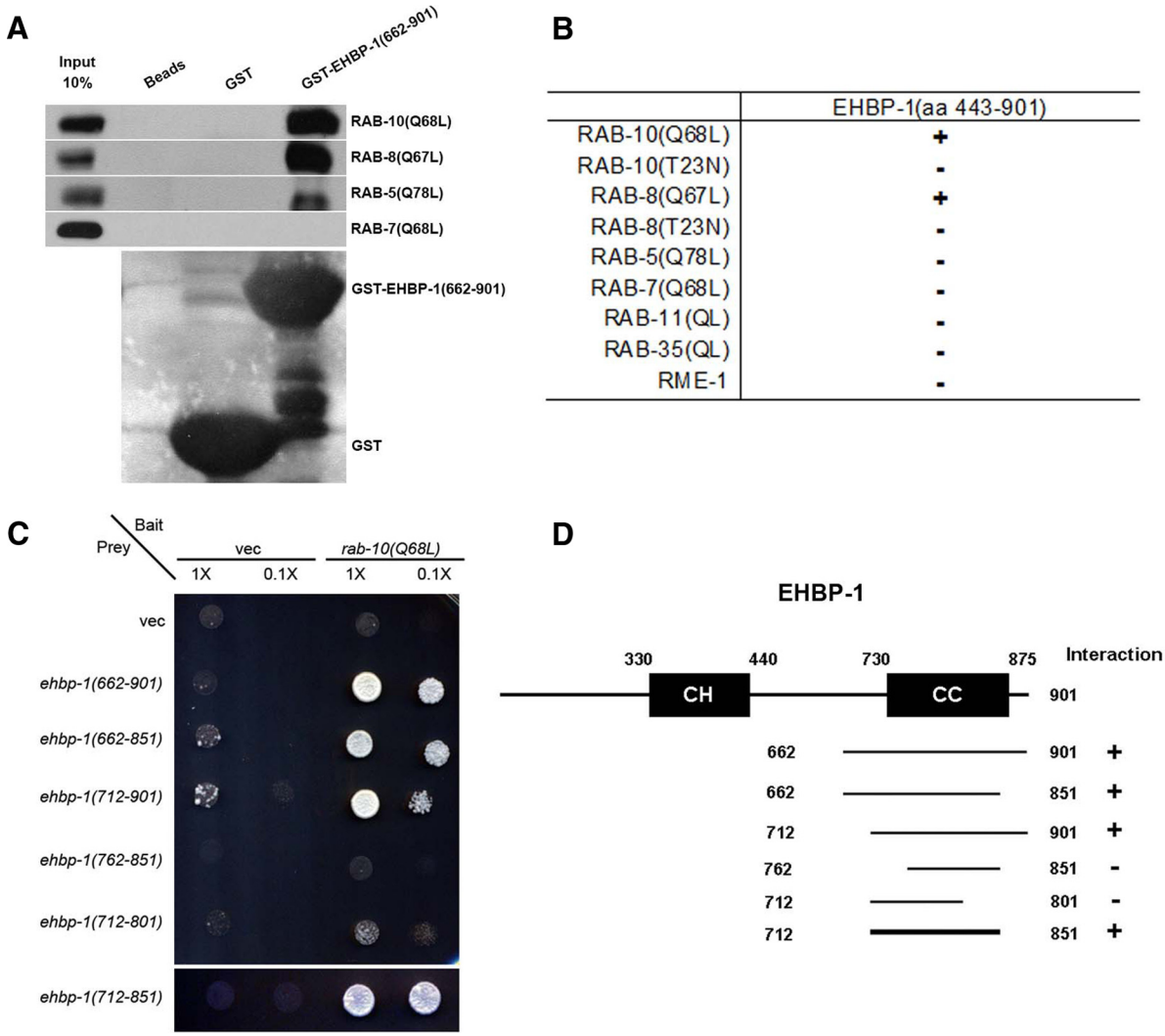

Figure 1. EHBP-1 physically interacts with RAB-10(Q68L) and RAB-8(Q67L). (A) Glutathione beads loaded with recombinant GST or GST-EHBP-1(aa 662–901) were incubated with in vitro–expressed HA-tagged RAB-5(Q78L), RAB-7(Q68L), RAB-8(Q67L), and RAB-10(Q68L) and then washed to remove unbound proteins. Bound proteins were eluted and analyzed by Western blot using anti-HA (top) or anti-GST (bottom) antibodies. Input lanes contain in vitro–expressed HA-tagged RABs used in the binding assays (10%). (B) Using EHBP-1 (aa 443–901) as bait, RME-1 and RABs with reported endosomal trafficking involvement were used as prey in yeast two-hybrid assays, including active RAB-5(Q78L), RAB-7(Q68L), RAB-8(Q67L), RAB-10(Q68L), RAB-11(Q70L), RAB-35(Q69L), and inactive RAB-8(QT23N) and RAB-10(QT23N). (C) RAB-10(Q68L) was expressed in a yeast reporter strain as a fusion with the DNA-binding domain of LexA (bait). EHBP-1–truncated forms were expressed in the same yeast cells as fusions with the B42 transcriptional activation domain (prey). Interaction between bait and prey was assayed by complementation of leucine auxotrophy (LEU2 growth assay). Colonies were diluted in liquid and spotted on solid growth medium directly or after further 0.1× dilution. (D) Schematic representations of EHBP-1 domains and the truncated fragments used in yeast two-hybrid analysis. Protein domains are displayed as dark boxes above protein sequence used in the study (shown as dark lines). Amino acid numbers are indicated.

are absent in invertebrate Ehbp1 homologues (Supplemental Figure S3A, highlighted in pink). The acquisition of EHD-binding capacity through NPF-motifs may represent a vertebrate innovation in an otherwise ancient protein family.

EHBP-1 Is Widely Expressed in C. elegans

RAB-10 has been shown to be ubiquitously expressed in *C. elegans* (Chen *et al.*, 2006). To determine the expression pattern and subcellular localization of EHBP-1, we established transgenic lines expressing an EHBP-1-GFP fusion protein, driven by *ehbp-1* upstream sequences (the predicted promoter region). EHBP-1-GFP fusion proteins were expressed in all somatic *C. elegans* tissues, including the pharynx and nerve ring, body-wall muscles, seam cells, intestine, oviduct sheath cell, and spermatheca (Figure 2, A–F). Thus EHBP-1 has the potential to interact with RAB-10 in all tissues. The EHBP-1-GFP fusion protein was localized in a punctate or tubular pattern in most tissues. In the intestine, EHBP-1-GFP was localized to both the apical and basolateral plasma membranes (Figure 2E). Near basolateral membranes, EHBP-1-GFP labels distinct cytoplasmic puncta resembling endosomes ranging in size from 0.5 to 1.0 μm (Figure 2D). In addition to punctate structures, EHBP-1-GFP also labeled tubular structures close to the basolateral plasma membrane of the intestine (Figure 2D).

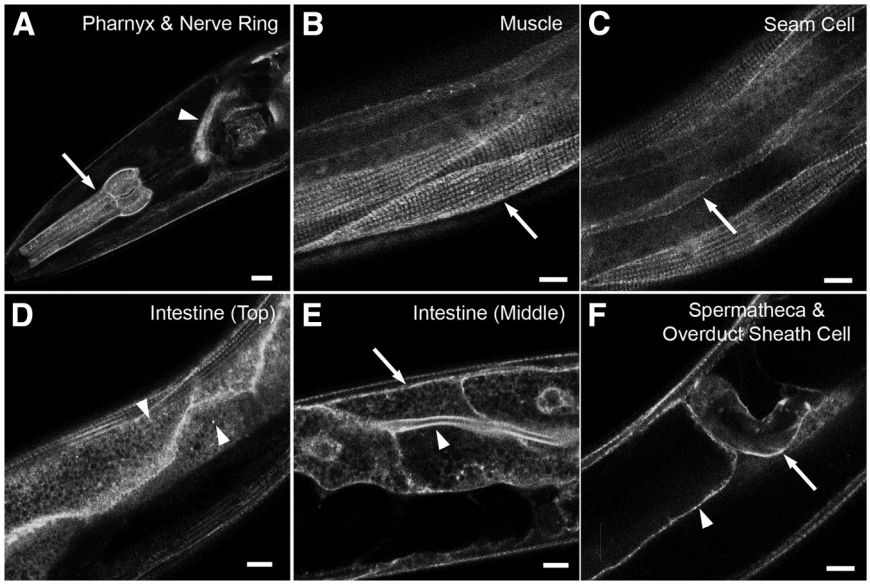

Figure 2. EHBP-1 is broadly expressed in *C. elegans*. Confocal images of EHBP-1-GFP transgene expression driven by the *ehbp-1* promoter. Tissue-specific expression was observed as follows: (A) pharynx (arrows), nerve ring (arrowhead); (B) myofilament of body-wall muscle (arrows); (C) seam cells (arrows); (D) intestine (Top); (E) intestine (Middle); arrows indicate the basolateral intestinal membranes, and arrowheads indicate the apical intestinal membranes and basolateral cytoplasmic puncta; (F) spermatheca (arrowheads) and oviduct sheath cells plasma membrane (arrows). Scale bar, 10 μm.

EHBP-1 Is Associated with Endosomes But Not Golgi in the Intestine

To determine where EHBP-1 is normally localized and to help test the hypothesis that EHBP-1 functions with RAB-10 in endocytic recycling, we performed a series of colocalization studies in the intestinal cells of living animals, comparing functional GFP-tagged EHBP-1 with a set of RFP-tagged endosomal markers described previously (Chen *et al.*, 2006). We observed the highest degree of colocalization of EHBP-1-GFP with RFP-RAB-10– and RFP-RAB-8–labeled endosomal puncta in the intestine (Figure 3, B–C). In polarized MDCK cells, Rab10 labels the common recycling endosome, and our previous work in *C. elegans* had indicated a function for RAB-10 in transport between basolateral early and recycling endosomes (Babbey *et al.*, 2006; Chen *et al.*, 2006). Rab8 has also been reported to regulate endocytic recycling in mammals, affecting the recycling of clathrin-independent cargos such as MHCI as well as clathrin-dependent cargo Tf (Hattula *et al.*, 2006). In the *C. elegans* intestine, we find that RFP-RAB-10 and GFP-RAB-8 colocalize extensively (Supplemental Figure S4, A–B). Closer examination showed that EHBP-1 colocalized with RAB-10 and -8 on punctate endosomal membranes. EHBP-1 also localized to tubular elements associated with the puncta and the plasma membrane (see Figure 6D). These results are consistent with EHBP-1 functioning with RAB-10 and/or -8 in vivo.

EHBP-1 occasionally colocalized with basolateral recycling endosome marker RME-1 (Figure 3, D–D″), as we had found previously for RAB-10 (Chen *et al.*, 2006). EHBP-1-GFP also occasionally overlapped with the early endosome marker RFP-RAB-5, but the EHBP-1-GFP–labeled structures more often localized near RFP-RAB-5 puncta rather than overlapping with them directly (Figure 3, A–A″). EHBP-1-GFP was not found to colocalize with the apical recycling marker RFP-RAB-11 or the Golgi marker MANS-RFP (Figure 3, E–F″). Taken together these results indicate that EHBP-1 is enriched on endosomes, where it could potentially interact with RAB-10 and -8 to regulate endosome-to-plasma membrane transport of cargo.

Loss of EHBP-1 Causes Endocytic Recycling Defects

Loss of RAB-10 results in dramatic endocytic trafficking defects in the *C. elegans* intestine (Chen *et al.*, 2006). One of the most obvious phenotypes observed in RAB-10 loss-of-function animals is the formation of grossly enlarged intestinal endosomes that are filled with fluid-phase markers taken up from the basolateral surface (Fares and Greenwald, 2001; Chen *et al.*, 2006). To determine if EHBP-1 shares some functions with RAB-10 in vivo, we first analyzed the intestines of animals depleted of EHBP-1 by RNAi-mediated knockdown or of animals containing a deletion allele of *ehbp-1* obtained from the National Bioresource Project for the Experimental Animal "Nematode *C. elegans*" in Japan. This *ehbp-1* mutant allele, *tm2523*, deletes 503 base pairs of genomic DNA corresponding to portions of the fifth and sixth exons and is predicted to place all coding regions downstream of the deletion out of frame, effectively truncating any remaining expressed protein after amino acid 302.

ehbp-1(RNAi) animals were slow growing and produced fewer progeny than control animals, whereas *ehbp-1(tm2523)* animals often arrested as larvae, and animals that reached adulthood were sterile (see below). *ehbp-1(RNAi)*-treated animals contained grossly enlarged intestinal endosomes that could be filled with a signal sequence–modified form of GFP (ssGFP) that is secreted from body-wall muscle cells (Fares and Greenwald, 2001), a phenotype very similar to that produced by *rab-10* loss-of-function mutants or *rab-10(RNAi)* (Figure 4, B and D; Chen *et al.*, 2006). Such vacuolated structures were also visible in the intestine of homozygous *ehbp-1(tm2523)* mutant animals and could be rescued by intestine specific expression of EHBP-1-GFP (Supplemental Figure S4, C–D′). *ehbp-1* RNAi knockdown was considered effective because it blocked expression of EHBP-1-GFP transgenes in control experiments and produced a spectrum of phenotypes very similar to the *ehbp-1(tm2523)* deletion mutant. These results suggest that loss of EHBP-1, like loss of RAB-10, produces severe defects in basolateral endocytic recycling.

Cargo-specific Requirements for EHBP-1

To test the importance and specificity of EHBP-1 in cargo recycling, we assayed the effect of *ehbp-1* mutation on well-established recycling cargo proteins hTAC-GFP (CIE marker) and hTfR-GFP (CDE marker) in *ehbp-1* mutant animals (Chen *et al.*, 2006; Shi *et al.*, 2007). We previously found that loss of

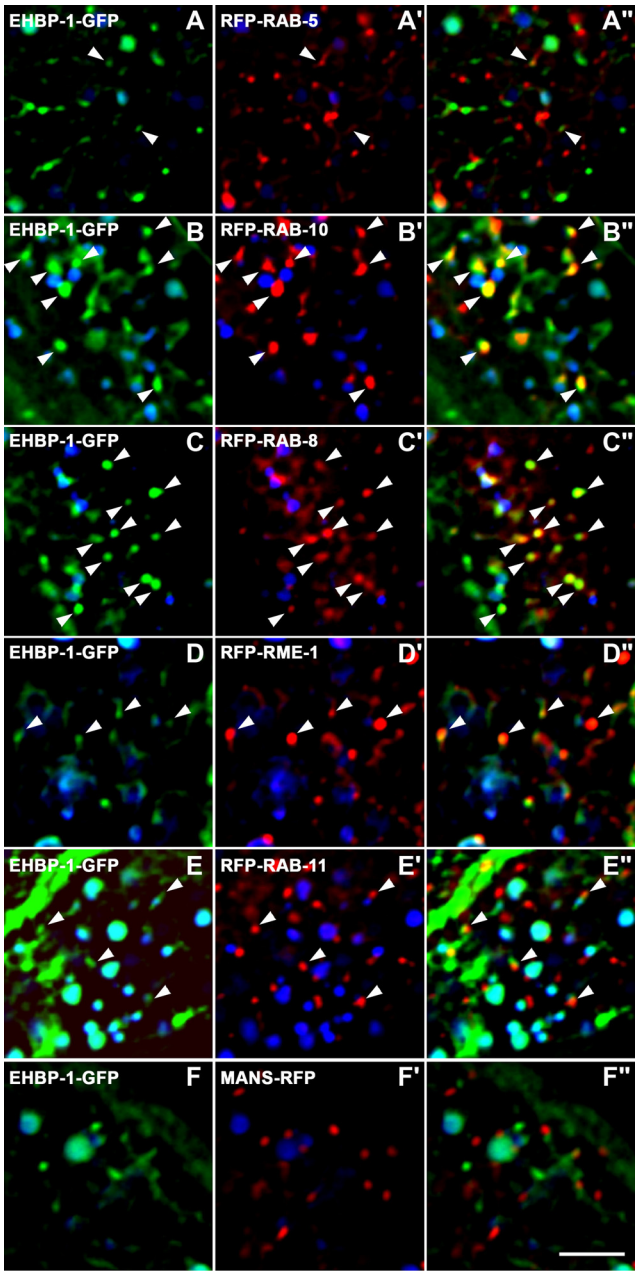

Figure 3. EHBP-1 colocalizes with RAB-10 and -8 on endosomes. All images are from deconvolved 3D image stacks acquired in intact living animals expressing GFP- and RFP-tagged proteins specifically in intestinal epithelial cells. (A–A″) Arrowheads, endosomes labeled by both EHBP-1-GFP and RFP-RAB-5. (B–B″) Arrowheads, endosomes labeled by both EHBP-1-GFP and RFP-RAB-10. (C–C″) Arrowheads, endosomes labeled by both EHBP-1-GFP and RFP-RAB-8. (D–D″) Arrowheads, endosomes labeled by both EHBP-1-GFP and RFP-RME-1. (E–E″) Arrowheads, EHBP-1-GFP–positive endosomes juxtaposed to RFP-RAB-11–labeled structures. (F–F″) EHBP-1-GFP does not colocalize with Golgi marker Mannosidase-RFP. In each image autofluorescent lysosome-like organelles can be seen in all three channels with the strongest signal in blue, whereas GFP appears only in the green channel and RFP only in the red channel. Signals observed in the green or red channels that do not overlap with signals in the blue channel are considered bone fide GFP or RFP signals, respectively. Scale bar, 10 μm.

RAB-10 caused dramatic intracellular accumulation of hTAC-GFP, consistent with a defect in hTAC recycling (Chen *et al.*, 2006). Loss of RAB-10 had only minor effects on hTfR-GFP (Chen *et al.*, 2006). These results suggested a cargo-specific role for RAB-10 in the recycling pathway.

In *ehbp-1(tm2523)* mutant animals, hTAC-GFP accumulated dramatically within the intestinal cells in intracellular tubules and enlarged puncta (Figure 4, F and K), very similar to the phenotype observed in *rab-10* mutants (Figure 4, G and K). hTfR-GFP localization appeared unperturbed in *ehbp-1(tm2523)* mutant animals, suggesting that like RAB-10, EHBP-1 affects recycling in a cargo-specific manner (Figure 4, I–K). Consistent with the direct action of EHBP-1 on endosomes transporting hTAC, we found a high degree of colocalization between EHBP-1-mCherry and hTAC-GFP on intracellular tubules and puncta (Supplemental Figure S5, A–A″).

Although overexpression of full-length EHBP-1-mCherry did not overtly affect the localization of hTAC-GFP, we found that overexpression of a truncated form of EHBP-1(aa1–711), lacking the RAB-10–interacting coiled-coil domain, induced dominant negative phenotypes including overaccumulation of intracellular hTAC-GFP and the formation of grossly enlarged intestinal vacuoles similar to those observed in *ehbp-1* loss-of-function mutants (Supplemental Figure S5, C–F). Colocalization studies showed that the truncated form of EHBP-1(aa1–711) colocalizes with hTAC-GFP on the accumulated intracellular structures (Supplemental Figure S5, B–B″).

EHBP-1 Is Important for Endosome Morphology

Our previous work indicated that the grossly enlarged endosomes in *rab-10* mutants are labeled by the early endosome marker GFP-RAB-5, but not by the basolateral recycling endosome marker GFP-RME-1. In fact, *rab-10* mutants extensively overaccumulate GFP-RAB-5 labeled early endosomes of all sizes and display abnormal localization of the recycling endosome marker GFP-RME-1. In *rab-10* mutants GFP-RME-1 is more diffusely distributed, with the remaining GFP-RME-1 labeled structures being larger, fewer in number, and displaying a pronounced loss of their normal tubular morphology (Chen *et al.*, 2006). *ehbp-1* mutants displayed very similar endosomal defects, including increased GFP-RAB-5 labeling and loss of GFP-RME-1–labeled recycling endosome tubular morphology (Figure 5, A–F, quantified in G and H). In contrast, there was no effect on the subcellular localization or number of RAB-11-labeled apical recycling endosomes in *ehbp-1* mutants (Supplemental Figure S6).

These results suggest that EHBP-1 and RAB-10 function at a similar step in endocytic transport, upstream of RME-1. Consistent with the idea that RME-1 functions downstream of RAB-10, we found that in *rme-1(b1045)* mutants the average intensity of GFP-RAB-10–labeled endosomes increased by about threefold (Figure 6, A, C, and H). This result suggests a blockage of the recycling pathway downstream of RAB-10 in cells lacking RME-1. We also found that the morphology of EHBP-1-GFP–labeled structures was perturbed in *rme-1* mutants. EHBP-1-GFP localization appeared less tubular, with abnormal accumulation in patches and enlarged puncta (Figure 6, D, F, and I). Lack of RME-1 did not appear to affect the association of EHBP-1-GFP with membranes however.

EHBP-1 Controls the Localization of RAB-10

In many cases proteins that interact with GTP-bound Rabs are effector proteins, and such effectors are often localized and/or activated by interaction with the Rab protein (Stenmark, 2009). To determine if RAB-10 and EHBP-1 display such a relation-

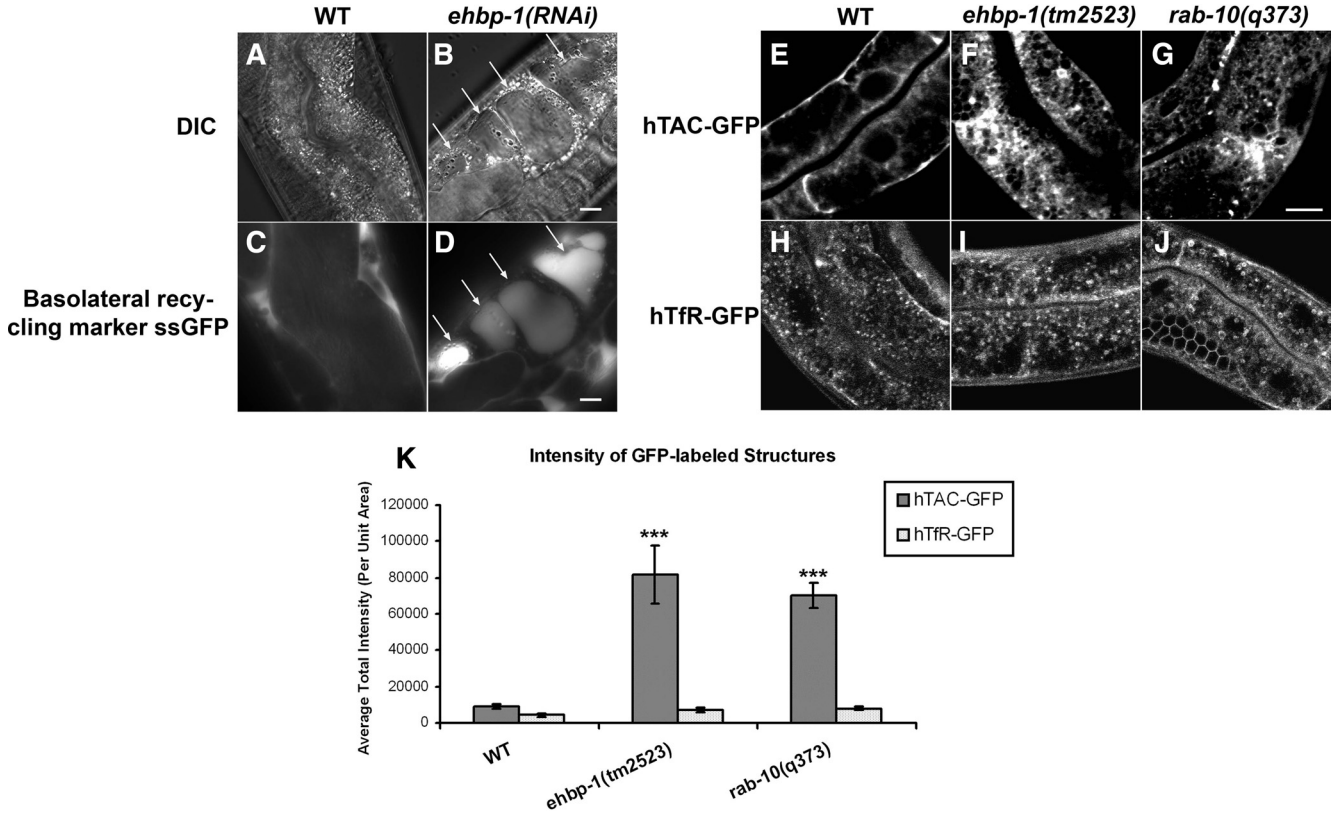

Figure 4. Loss of EHBP-1 induces endocytic recycling defects in the *C. elegans* intestine. (A and B) Nomarski images of the intestines in wild-type and *ehbp-1(RNAi)* animals. Large transparent vacuoles were found in the intestines of *ehbp-1(RNAi)* animals (B). Arrows indicate the positions of vacuoles. (C and D) Intestinal endocytosis of the basolateral recycling marker ssGFP in the wild-type and *ehbp-1(RNAi)* animals. Compared with wild-type animals, little ssGFP accumulates because of efficient recycling back to the body cavity (C), *ehbp-1(RNAi)* animal-specific vacuoles were filled with basolaterally endocytosed ssGFP (D, arrows). A *cup-4(ar494)* mutation was also included in the strain shown in C and D to impair coelomocyte function and increase steady-state levels of secreted ssGFP in the body cavity. (E–K) Confocal images of the worm intestine expressing GFP-tagged cargo proteins that recycle via the recycling endosome, the human transferrin receptor (hTfR-GFP) and the IL-2 receptor alpha chain (hTAC-GFP) in wild-type, *ehbp-1(tm2523)*, and *rab-10(q373)* mutant animals. Compared with wild-type animals (E), hTAC-GFP accumulates significantly on the intestinal cytosolic endosomal structures in *ehbp-1(tm2523)* and *rab-10(q373)*, about eightfold and sevenfold increase of the average total GFP intensity, respectively (F, G, and K). hTfR-GFP was not affected in *ehbp-1(tm2523)* and *rab-10(q373*) mutants (I, J, and K). Error bars, SEM (n = 18 each, six animals of each genotype sampled in three different regions of each intestine defined by a 100 × 100-pixel box positioned at random). Significant difference in the one-tailed Student's *t* test (***$p < 0.001$). Scale bar, 10 μm.

ship, we assayed for changes in the localization of EHBP-1-GFP in a *rab-10* mutant background. In the absence of RAB-10, the morphology of EHBP-1-GFP–labeled structures was perturbed, but EHBP-1 localization to membranes was not significantly affected (Figure 6, D and E, and quantified in I). EHBP-1-GFP localization appeared less tubular, with abnormal accumulation in patches, vacuoles, and enlarged puncta (Figure 6, D and E, and Supplemental Figure S7C). RNAi-mediated knockdown of RAB-8 did not perturb the morphology of EHBP-1-GFP–labeled structures (Supplemental Figure S7B). In addition, *rab-8(RNAi)* in a *rab-10* mutant background did not further disrupt EHBP-1-GFP endosomal morphology or membrane localization beyond that already observed in *rab-10* mutants alone (Supplemental Figure S7, C and D). These results suggest that although RAB-10 is important for the morphology of EHBP-1 associated endosomes, neither RAB-10 nor -8 is required for the EHBP-1 endosomal recruitment.

We also performed the converse experiment, testing for changes in GFP-RAB-10 and GFP-RAB-8 localization in animals lacking EHBP-1. Surprisingly, we found that GFP-RAB-10 was much more diffusive in the cytosol of *ehbp-1(tm2523)* mutants than in control animals (Figure 6, A and B). The intensity of GFP-RAB-10–labeled puncta was reduced by ~20-fold in *ehbp-1* mutants (Figure 6H). The increased diffusion and reduced intensity of GFP-RAB-10 endosomal labeling suggests that EHBP-1 functions upstream of RAB-10, promoting the association of RAB-10 with endosomes. Unlike GPP-RAB-10, we found that GFP-RAB-8–labeled structures overaccumulated in *ehbp-1(RNAi)* animals (Supplemental Figure S8, B and E). Furthermore, GFP-RAB-8–labeled structures also overaccumulated in *rab-10(q373)* mutants (Supplemental Figure S8, C and E). This behavior of the RAB-8–marked endosomes is very similar to that we observed with RAB-5–labeled endosomes and is the opposite of the observed effect on GFP-RAB-10. These data suggest that neither RAB-8 nor -5 requires EHBP-1 for endosomal recruitment. Rather these results indicate that RAB-8 and -5 are present on the endosomes that overaccumulate in the absence of RAB-10/EHBP-1–dependent recycling.

EHBP-1 Regulates GLR-1 Glutamate Receptor Trafficking

In addition to its role in the intestinal epithelium, *C. elegans* RAB-10 has also been reported to regulate the endocytic recycling of the AMPA-type glutamate receptor GLR-1,

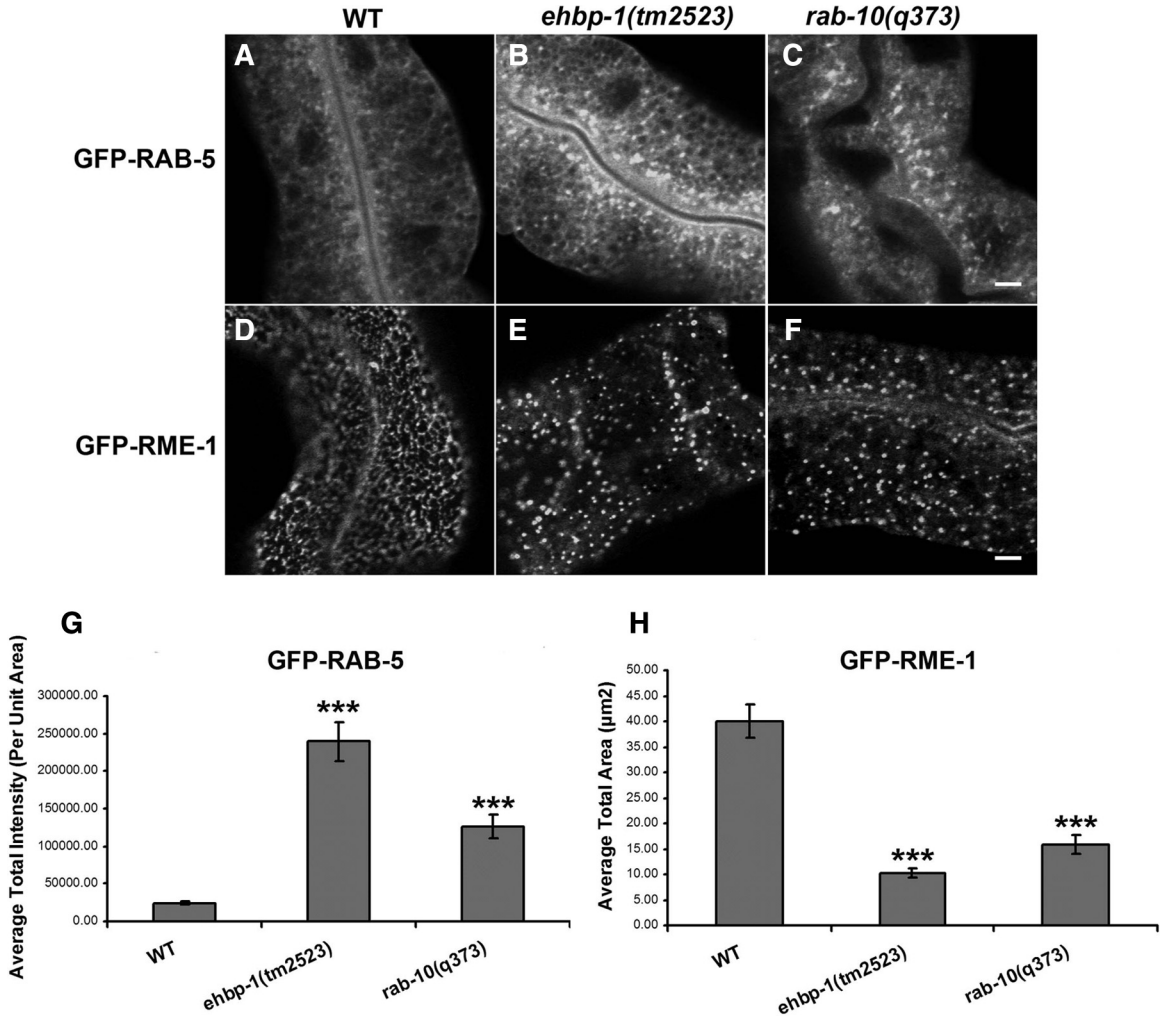

Figure 5. Accumulation of RAB-5–positive early endosomes and disrupted RME-1–positive tubular recycling structures in *ehbp-1(tm2523)* and *rab-10(q373)* mutants. Representative confocal images are shown for GFP-RAB-5 (A–C) and GFP-RME-1 (D–F). Approximate 10- and 5-fold average total intensity increase of GFP-RAB-5 were observed in *ehbp-1(tm2523)* and *rab-10(q373)* mutants (A–C and G). To quantify the RME-1–labeled structures disruption, average total area of positive GFP labeling per unit area was measured (H). Error bars, SEM (n = 18 each, six animals of each genotype sampled in three different regions of each intestine). Significant difference in the one-tailed Student's *t* test (***$p < 0.001$). Scale bar, 10 μm.

which is localized to synapses and controls the command interneuron circuit that mediates reversal behavior while animals forage (Hart *et al.,* 1995; Maricq *et al.,* 1995; Glodowski *et al.,* 2007). To determine whether, like RAB-10, EHBP-1 has a similar role in GLR-1 trafficking, we introduced a transgene expressing a full-length GLR-1-GFP chimeric protein into *ehbp-1* mutants (Rongo *et al.,* 1998). In control animals, GLR-1-GFP is localized to small (~0.5 μm) punctate structures that colocalize with other postsynaptic proteins along ventral cord neurites (Figure 7A; Rongo *et al.,* 1998; Burbea *et al.,* 2002). In both *rab-10* and *ehbp-1* mutant animals, we found an abnormal accumulation of GLR-1-GFP in elongated (~2–5 μm) accretions along the ventral cord neurites (Figure 7, B and C). These accretions are thought to be receptors trapped in internal compartments, most likely endosomes (Glodowski *et al.,* 2007; Chun *et al.,* 2008; Park *et al.,* 2009). We quantified the magnitude of the effect of *rab-10* and *ehbp-1* mutations on GLR-1 localization by classifying localized GLR-1-GFP into either small puncta or long accretions based on their size and morphology. Both mutants had elevated numbers of GLR-1 accretions (Figure 7D), with a mean size greater than that found for the rare accretion seen in wild type (Figure 7E). In contrast, *ehbp-1* and *rab-10* mutants contained fewer than wild-type numbers of small GLR-1-GFP puncta, which are thought to be receptors clustered at postsynaptic elements (Figure 7F; Rongo *et al.,* 1998; Burbea *et al.,* 2002). In contrast to *ehbp-1* and *rab-10* mutants, *rab-8* mutants displayed only very mild perturbation of GLR-1-GFP puncta and accretion size and displayed normal accretion and puncta number (Supplemental Figure S9, A–F).

The change in GLR-1-GFP localization in *ehbp-1* mutants could be due to defects in synapse formation. To test this possibility, we introduced a transgene expressing synaptic vesicle marker SNB-1-GFP (synaptobrevin), which labels synaptic terminals in the interneurons, into *ehbp-1* mutants (Nonet *et al.,* 1998; Rongo *et al.,* 1998). The number and distribution of SNB-1-GFP–labeled structures were similar in both wild-type and *ehbp-1* mutant animals (Figure 7, G–I), indicating that the observed defects in GLR-1 localization are unlikely to be due to gross defects in synapse formation.

If *ehbp-1* mutations prevent the recycling of GLR-1 and instead result in GLR-1 accumulating in internal accretions,

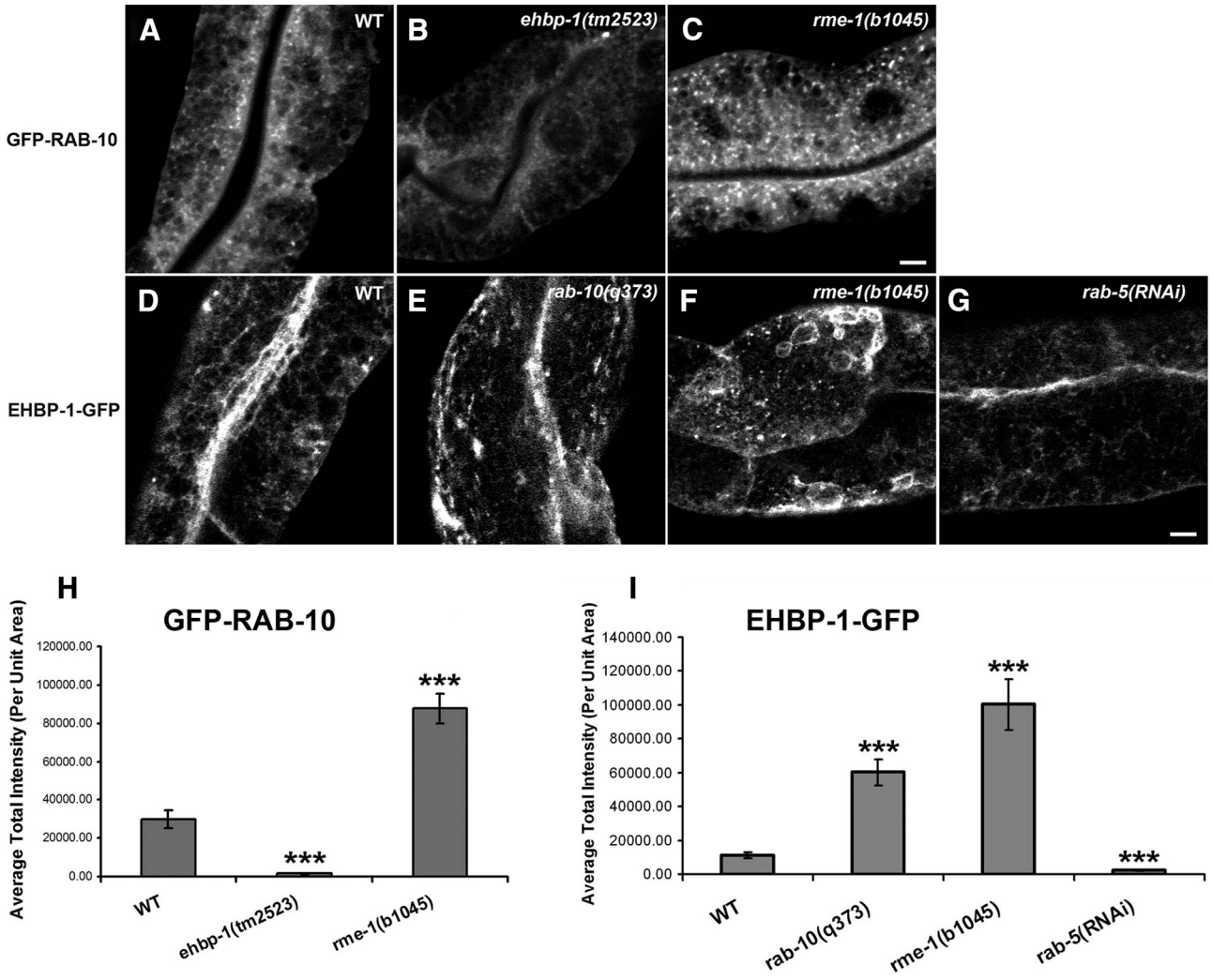

Figure 6. RAB-10–positive endosomal labeling dramatically decreases in *ehbp-1(tm2523)* mutants, but accumulate significantly in *rme-1(b1045)* mutants (A–C and H). Representative confocal images of wild-type animals and mutants are shown for GFP-RAB-10 (A–C) and average total intensity of GFP-RAB-10 in unit area was quantified in H. The number of EHBP-1–labeled endosomal structures were significantly increased in *rab-10(q373*) and *rme-1(b1045)* mutants (D–F and I), but *rab-5* RNAi knockdown significantly diminished labeling of EHBP-1 on tubular and punctuate structures (G and I). Representative confocal images of wild-type animals and mutants are shown for EHBP-1-GFP (D–G), and average total intensity of EHBP-1-GFP in unit area was quantified in I. Error bars, SEM (n = 18 each, six animals of each genotype sampled in three different regions of each intestine). Significant difference in the one-tailed Student's *t* test (***$p < 0.001$). Scale bar, 10 μm.

then these mutations should result in corresponding GLR-1–mediated behavioral defects (Burbea *et al.*, 2002; Glodowski *et al.*, 2007). GLR-1 positively regulates spontaneous reversals in locomotion during foraging, and the frequency of these reversals provides a quantitative measure of GLR-1 activity (Zheng *et al.*, 1999; Mellem *et al.*, 2002). We measured the spontaneous reversal frequency of wild type, *glr-1* mutants, *rab-10* mutants, *ehbp-1* homozygous mutants, and *ehbp-1* heterozygotes (30 animals, 5-min trials). As previously described, *rab-10* mutants change direction at half the rate of wild-type animals, similar to the rate observed in *glr-1* null mutants (Glodowski *et al.*, 2007; Figure 7J). Like *rab-10* mutants, *ehbp-1* mutants reversed direction at a depressed rate. Unlike *rab-10* and *ehbp-1*, *rab-8* mutants displayed normal spontaneous reversal frequency (Supplemental Figure S9G).

Taken together, these results indicate that EHBP-1 and RAB-10 regulate the trafficking of GLR-1 from endosomal compartments within the neurites to synaptic membranes, whereas RAB-8 plays little or no role in this process.

As described above, RAB-10 and EHBP-1 can physically interact in vitro. To determine whether EHBP-1 and RAB-10 associate at similar compartments in the ventral cord neurites in vivo, we introduced transgenes that express EHBP-1-GFP and mRFP-RAB-10 in the interneurons via the *glr-1* promoter. We found extensive colocalization of EHBP-1-GFP and RFP-RAB-10 along the ventral cord neurites (Figure 7, K–M). These findings indicate that EHBP-1 and RAB-10 are largely present at the same subcellular structures along the ventral cord. Unlike RFP-RAB-10, RFP-RAB-8 was diffusely distributed throughout the neurites and failed to colocalize with GFP-EHBP-1 (Supplemental Figure S9H).

In *C. elegans* intestinal cells, EHBP-1 regulates RAB-10 subcellular localization. To test for a similar role in neurons, we assayed *ehbp-1* mutants for changes in GFP-RAB-10 localization in interneurons. Although GFP-RAB-10 is local-

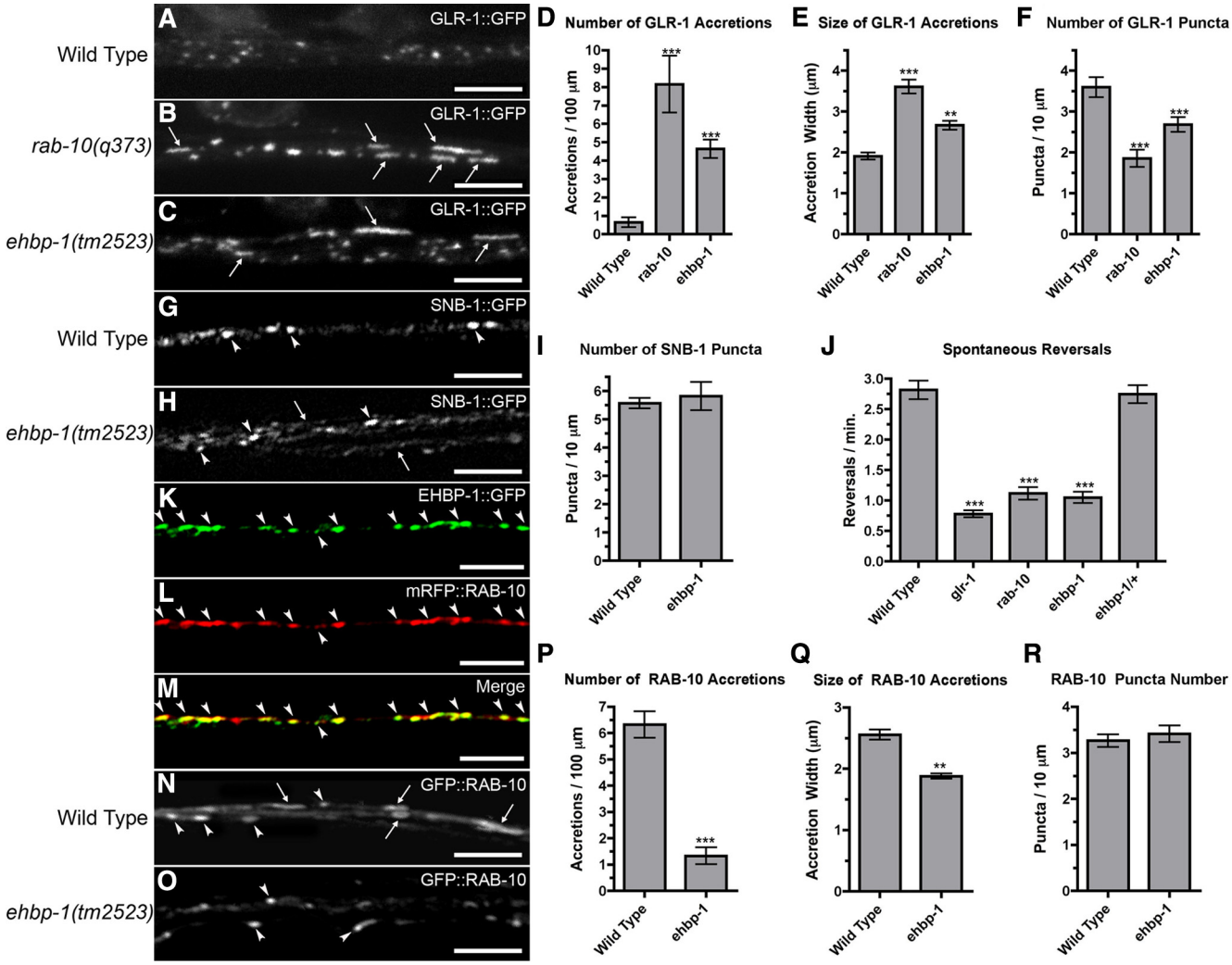

Figure 7. EHBP-1 regulates GLR-1 glutamate receptor trafficking. GLR-1-GFP fluorescence was observed along ventral cord neurites of (A) wild-type animals, (B) *rab-10(q373)* mutants, and (C) *ehbp-1(tm2523)* mutants. In wild-type animals, GLR-1-GFP is localized to small (~0.5 μm) synaptic puncta. By contrast, *ehbp-1* mutants, like *rab-10* mutants, accumulate GLR-1-GFP in elongated (~2–5 μm) accretions (arrows). The mean number (per 100 μm of ventral cord; D) and size (length in μm; E) of GLR-1-GFP accretions is plotted. The mean number of GLR-1-GFP puncta (per 100 μm of ventral cord; F) is also plotted. Presynaptic marker SNB-1-GFP shows similar localization to puncta along the ventral cord of wild-type (G) and *ehbp-1* mutant (H) animals; the mean number (I) is indicated. Occasionally some neurites are found outside of the main ventral cord fascicle of *ehbp-1* mutants (arrow in H), although this does not appear to grossly affect synapse formation. (J) The mean spontaneous reversal frequency (number of reversals per minute over a 5-min period) is plotted for the given genotype. EHBP-1-GFP (K) and mRFP-RAB-10 (L) are colocalized to subcellular compartments (arrowheads) in the ventral nerve cords. (M) Merged image. (N) GFP-RAB-10 is localized to small puncta (arrowheads) and large accretions (arrows) along the ventral cord of wild-type animals, but is only found in puncta in *ehbp-1* mutants (O), indicating that EHBP-1 regulates RAB-10 subcellular localization. The number per ventral cord length (P) and mean size (Q) of GFP-RAB-10 accretions, as well as the number of GFP-RAB-10 puncta (R) are plotted. Scale bar, 5 μm. Error bars , SEM. n = 15–20 animals for each genotype. *$p < 0.05$, **$p < 0.01$, ***$p < 0.001$ by analysis of variance (ANOVA) followed by Dunnett's multiple comparison to wild type (D–F and J) or by *t* test (P and Q).

ized at both large accretions and small punctae along the ventral nerve cord in control animals (Figure 7N), GFP-RAB-10 is only localized to small puncta in *ehbp-1* mutants (Figure 7O). In *ehbp-1* mutant animals, the average number of GFP-RAB-10–containing accretions was reduced dramatically (approximately sixfold lower than that in control animals; Figure 7P), and the mean size of the accretions was also reduced (Figure 7Q). The number of small GFP-RAB-10 puncta remained the same (Figure 7R). Taken together, these results indicate that, similar to what was observed in the intestinal cells, EHBP-1 regulates the subcellular localization of RAB-10 in neurons.

EHBP-1 Is Required in the Germline

As mentioned earlier, we found that adult *ehbp-1(tm2523)* mutant animals are completely sterile (0 eggs produced, n = 18 adult hermaphrodites). The sterile adults have abnormally small gonads and completely lack the characteristic row of large squared-off oocyte cells in the proximal gonad region (Figure 8, A and E, arrows). This suggests a defect in oocyte growth and/or differentiation in these animals. Although such a phenotype might be explained by severe membrane-trafficking defects in the germline cells, this phenotype cannot be completely explained simply by loss of RAB-10 or -8 function, because neither the *rab-10* nor *-8*

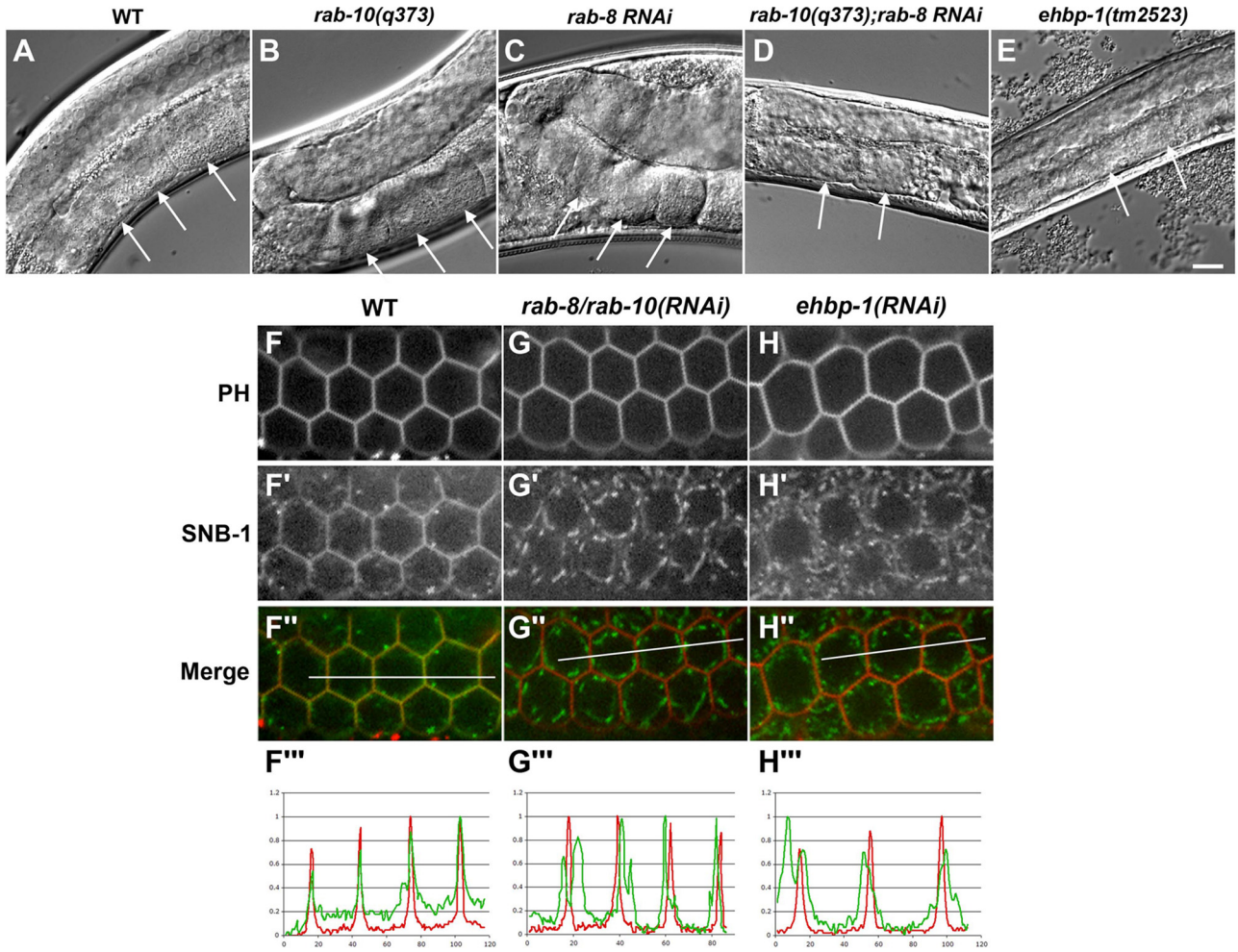

Figure 8. (A–E) Nomarski images of the gonads in wild-type, *rab-10(q373)*, *rab-8(RNAi)*, *rab-10(q373);rab-8(RNAi)*, and *ehbp-1(tm2523)* animals. Developmental defects of gonads were found in *rab-10(q373);rab-8(RNAi)* animals and *ehbp-1(tm2523)* mutants (D and E). Arrows indicate the normal large squared-off oocyte cells in the proximal gonad region (A–C) and the lack of the characteristic row of oocyte cells in the proximal gonad regions (D and E). Scale bar, 10 μm. (F–H‴) Depletion of EHBP-1 or codepletion of RAB-8 and -10 result in a similar defect in germline secretion. GFP-SNB-1 localized mostly to the plasma membrane of developing compartments in the germline and colocalized with mCherry-PH at steady state (F–F″). Line-scan analysis showed that fluorescence intensity of GFP-SNB-1 and mCherry-PH peaked at identical points (F‴). RNAi depletion of RAB-8 and -10 caused a defect in the localization of GFP-SNB-1 at the plasma membrane (G–G‴). RNAi depletion of EHBP-1 caused a similar defect in GFP-SNB-1 delivery to the plasma membrane (H–H‴).

mutant is sterile; however, each single mutant does display a reduced brood size. We measured *rab-10* mutant brood size as 162 ± 10 (n = 18) and *rab-8* mutant brood size as 152 ± 4 (n = 18), compared with wild-type N2 controls that displayed a brood size of 280 ± 12 (n = 18).

Thus we sought to determine if the sterile phenotype might be explained by loss of RAB-8 function, in addition to RAB-10 function, in the *ehbp-1* mutant germ cells. This was suggested by the findings that EHBP-1 can physically interact with RAB-8 in addition to RAB-10, that RAB-8 and -10 are very similar to each other at the sequence level, and previous RNAi evidence that RAB-8 and -10 possess an essential overlapping function in the germline (Audhya *et al.*, 2007). There have also been suggestions of redundancy in this Rab pair in mammalian MDCK cells (Schuck *et al.*, 2007). Thus we compared the germline phenotype of *ehbp-1* mutants with that of animals depleted of RAB-8 or of animals depleted of both RAB-8 and -10. We found that although RNAi-mediated depletion of RAB-8 did not produce sterility in an otherwise wild-type background, RNAi-mediated depletion of RAB-8 in a *rab-10* mutant background produced sterile adult phenotypes that strongly resembled *ehbp-1* mutant animals (Figure 8, D and E, and Supplemental Figure S10, arrows).

Given the poor growth of the germline, and the abnormal oocytes in particular, the typical assay used to measure endocytic transport in the germline—uptake of GFP-tagged yolk proteins by oocytes—did not appear appropriate. In addition, our previous work indicated that oocytes of nearly normal size are produced in animals with severe defects in oocyte endocytosis, whereas defects in secretion frequently lead to small and abnormal oocytes (Grant and Hirsh, 1999; Balklava *et al.*, 2007). To identify the underlying defect we focused on the oocyte precursors located between the transition zone and the bend in the gonad arm, assaying effects of loss of EHBP-1, RAB-10, and/or RAB-8 on the localization of a secreted transmembrane SNARE protein, SNB-1 (boxed region in the diagram, Supplemental Figure S11). Although SNB-1 is best known as a neuronal protein found mainly found in synaptic vesicles, it is also normally expressed in

the germline (Sato *et al.*, 2008a). At steady state, GFP-SNB-1, like endogenous SNB-1 (Sato *et al.*, 2008a), localized mostly to the plasma membrane of developing compartments in the germline, although a subpopulation could also be found on punctate structures that likely correspond to secretory vesicles and endosomes (Figure 8F′ and data not shown). The accumulation of GFP-SNB-1 on the plasma membrane was confirmed by colocalization studies with an mCherry fusion to the PH domain derived from rat PLC1δ, which binds specifically to the plasma membrane-localized lipid, phosphatidylinositol 4,5-bisphosphate (Figure 8, F–F″). Line-scan analysis showed that the fluorescence intensities of GFP-SNB-1 and mCherry-PH peaked at identical points, illustrating a high degree of colocalization (Figure 8F‴). Codepletion of RAB-8 and -10 caused a striking defect in the accumulation of GFP-SNB-1 at the plasma membrane. Instead, the SNARE protein accumulated almost exclusively on internal punctate structures and failed to colocalize with the plasma membrane mCherry-PH marker (Figure 8, G–G‴). Depletion of EHBP-1 caused a similar defect in GFP-SNB-1 transport to the plasma membrane (Figure 8, H–H‴). Taken together, these results indicate that RAB-8 and -10 function redundantly in the secretory pathway of *C. elegans* germ cells and further suggest that EHBP-1 functions with RAB-8 and -10 in this process.

DISCUSSION

Here we present the first functional studies of *ehbp-1* mutant animals and demonstrate an important relationship between EHBP-1 with RAB-10 during endocytic recycling. We show that a predicted coiled-coil domain in the C-terminus of EHBP-1 binds directly to active GTP-bound RAB-10, that a functional EHBP-1-GFP fusion protein colocalizes with RFP-RAB-10 in epithelial cells and neurons, and that animals lacking EHBP-1 or RAB-10 share a specific set of endosomal defects, miss-sort cargo proteins in a similar manner, and display similar defects in organismal behavior. The RAB-10-like phenotypes found in *ehbp-1* mutants appear to result from a failure to efficiently recruit RAB-10 to endosomal membranes. However, in some respects, loss of EHBP-1 more severely impacts *C. elegans* development as compared with the loss of RAB-10, more closely resembling the defects found in animals lacking both RAB-10 and RAB-8, to which EHBP-1 can also bind.

The finding that EHBP-1 is important for RAB-10 membrane recruitment is unexpected, because EHBP-1 appears to interact with the GTP-bound form of RAB-10. Membrane recruitment of Rabs is most commonly associated with Rab guanine nucleotide exchange factors (GEFs), but GEFs interact with the GDP-bound or nucleotide-free forms of the Rab and promote GDP/GTP exchange. Proteins that bind to GTP-bound Rabs are typically thought of as Rab effectors, and Rab effectors are typically recruited to the membrane by the Rab GTPase, and not vice versa as was observed in this case. However, there is an interesting recent precedent for this type of interaction. While this manuscript was in preparation, an article by Sharma *et al.* (2009) showed that mammalian MICAL-L1, identified as a Rab8(GTP) binding partner, functions as an upstream regulator of Rab8 that is important for the association of Rab8 with endosomal membranes. This study is also particularly relevant because MICAL-L1 has a domain structure somewhat similar to EHBP-1, including a central CH-domain and a C-terminal Rab-binding domain predicted to adopt a coiled-coil structure. Mammalian cells express Ehbp1 in addition to several different MICAL proteins, and the MICAL proteins all engage various members of the Rab10/Rab8/Rab13 family to promote endocytic transport (Weide *et al.*, 2003; Yamamura *et al.*, 2008). EHBP-1 appears to be the only *C. elegans* protein bearing a similar domain structure to mammalian Ehbp1 and MICAL-L1 in the predicted worm proteome.

Mammalian Ehbp1 was originally identified in NIH3T3 cells as a binding partner of EHD1 and EHD2, members of the RME-1 family of ATPases (Guilherme *et al.*, 2004a; Guilherme *et al.*, 2004b). Likewise, MICAL-L1 was recently shown to bind to EHD1 (Sharma *et al.*, 2009). Mammalian Ehbp1 and MICAL-L1 contain N-terminal NPF sequences that bind to the C-terminal EH-domain of the EHD proteins. RME-1/EHD family proteins are ATPases that are thought to function as membrane tubulation and/or fission molecules on endosomes, possibly functioning in a manner analogous to the well-studied fission regulator Dynamin (Daumke *et al.*, 2007; Grant and Caplan, 2008; Pant *et al.*, 2009). The direct association of EHBP-1/MICAL-L1-type proteins with RME-1/EHDs does not appear to be evolutionarily conserved, however, because *C. elegans* EHBP-1 lacks NPF sequences, and we could not detect a physical interaction between RME-1 with EHBP-1. Rather, EHBP-1's effects on RME-1 localization appears to be indirect, mediated through regulation of RAB-10. EHBP-1 and RAB-10 function upstream of RME-1 at the basolateral early and/or recycling endosome in intestinal cells, affecting RME-1 localization to tubular membranes of the recycling endosome.

It is also interesting to note that in the 3T3 adipocyte model, siRNA-mediated depletion of Ehbp1 abolished the insulin-regulated endosome to plasma membrane transport of the glucose transporter Glut4 (Guilherme *et al.*, 2004b). Because mammalian Rab10 (in adipocytes) and mammalian Rab8 (in muscle cells) are now known to be important for Glut4 recycling in response to an insulin signal (Sano *et al.*, 2007; Randhawa *et al.*, 2008), it is reasonable to suspect that mammalian Ehbp1 might mediate its effects on Glut4 via interaction with Rab10 and/or Rab8.

In our study, we showed that EHBP-1 also physically interacts with RAB-8 in vitro and colocalizes with RAB-8 in vivo. Nevertheless, we noticed significant phenotypic differences upon loss of RAB-10 or -8 in various tissues. For instance, depletion of RAB-10 strongly affects EHBP-1 labeled endosome morphology in the polarized intestinal cells, an effect not seen upon knockdown of RAB-8 (Supplemental Figure S7). Likewise, loss of RAB-8 has very mild effects on GLR-1 localization in interneurons and has no effect on GLR-1–mediated behavior (Supplemental Figure S9, A–G). By contrast, in the nonpolarized germline cells, SNB-1 delivery to the PM was disrupted only upon simultaneous loss of RAB-10 and -8; no defect was observed upon loss of only one of these Rabs. These apparent tissue-specific differences in Rab function may have broader implications. Nonpolarized cells, such as oocytes, may have generally greater redundancy within their endocytic recycling pathways compared with polarized cells such as those of the intestine or nervous system. The increased complexity of basolateral versus apical, or dendritic versus axonal, transport in polarized cells may require greater specialization, and thus perhaps less redundancy, in such pathways. A recent study in the mouse suggested that Rab8 is important for apical transport in polarized enterocytes and also suggested that the same may be true of *C. elegans* RAB-8 (Sato *et al.*, 2007). This is also interesting in light of recent work indicating a Rab11/Rab8 cascade in cilia formation (Knodler *et al.*, 2010) and the known preference of Rab11 for apical recycling in polarized epithelia (Casanova *et al.*, 1999; Brown

et al., 2000). Thus one possibility is that in polarized cells like the intestinal enterocytes, RAB-8 and -10 function differentially in apical versus basolateral recycling, whereas in nonpolarized cells such as oocytes both pathways exist but function redundantly.

Rab family GTPases have been shown to function in the generation, maintenance, and membrane trafficking processes of intracellular compartments (Stenmark, 2009). Different Rab GTPases can coexist on the same compartment in distinct subdomains, and in some cases Rab cascades have been proposed (Sonnichsen *et al.*, 2000; Ortiz *et al.*, 2002). For instance Rab5 is thought to recruit activators of Rab7 to the endosome during endosome maturation, promoting entry of cargo into the degradative compartment and recycling of retromer-dependent cargo to the Golgi (Rink *et al.*, 2005). However, Rab5 also interacts with the recycling machinery that promotes transport to recycling endosomes. For instance, Rab5 binds to Rabenosyn-5, a protein that also interacts with recycling associated proteins Rab4 and EHD1 (Naslavsky *et al.*, 2004, 2006). *In vitro*, we observed a weak binding of EHBP-1 to RAB-5, albeit not as strong an interaction as was found with RAB-10 or -8. Interestingly, we observed that RNAi-mediated knockdown of RAB-5 resulted in poor recruitment of EHBP-1 to endosomal membranes (Figure 6, G and I). Conversely, loss of EHBP-1 caused the abnormally high accumulation of GFP-RAB-5, in parallel with a defect in proper recruitment of RAB-10. Thus, one possibility is that EHBP-1 interacts with RAB-5 and -10 sequentially, acting to promote the exchange of RAB-5 for RAB-10 on endosomes as they mature along the recycling pathway. Further analysis will be required to substantiate such a model.

The CH-domain of EHBP-1 is also interesting with regard to endosome function, as CH-domains are thought to interact with cytoskeletal elements. Classically CH-domains are thought to be actin-interaction modules, although recent work suggests that in some proteins CH-domains can interact with microtubules (Sjoblom *et al.*, 2008). Actin in particular is important for the recycling of CIE cargo such as TAC and MHCI, and EHBP-1 and RAB-10 are preferentially involved in the recycling of such cargo (Radhakrishna and Donaldson, 1997; Weigert *et al.*, 2004). Future analysis will be focused on determining if EHBP-1 helps to connect endosomes to cytoskeletal networks to promote endocytic recycling function.

ACKNOWLEDGMENTS

We thank Yuji Kohara (National Institute of Genetics, Japan) and Shohei Mitani (Tokyo Women's Medical University) for important reagents, and we thank Karen Oegema (Ludwig Institute for Cancer Research, San Diego, CA) for generously providing unpublished marker strains for this study. We thank Saumya Pant, Peter Schweinsberg, and Zui Pan for their generous advice and technical assistance. R.B. was supported by Aresty Research Center grant. This work was supported by National Institutes of Health (NIH) R01 NS42023 to C.R. This work was supported by NIH Grant GM067237 to B.D.G.

REFERENCES

Allaire, P. D., Marat, A. L., Dall'Armi, C., Di Paolo, G., McPherson, P. S., and Ritter, B. (2010). The Connecdenn DENN domain: a GEF for Rab35 mediating cargo-specific exit from early endosomes. Mol. Cell *37*, 370–382.

Ang, A. L., Folsch, H., Koivisto, U. M., Pypaert, M., and Mellman, I. (2003). The Rab8 GTPase selectively regulates AP-1B-dependent basolateral transport in polarized Madin-Darby canine kidney cells. J. Cell Biol. *163*, 339–350.

Ang, A. L., Taguchi, T., Francis, S., Folsch, H., Murrells, L. J., Pypaert, M., Warren, G., and Mellman, I. (2004). Recycling endosomes can serve as intermediates during transport from the Golgi to the plasma membrane of MDCK cells. J. Cell Biol. *167*, 531–543.

Audhya, A., Desai, A., and Oegema, K. (2007). A role for Rab5 in structuring the endoplasmic reticulum. J. Cell Biol. *178*, 43–56.

Babbey, C. M., Ahktar, N., Wang, E., Chen, C. C., Grant, B. D., and Dunn, K. W. (2006). Rab10 regulates membrane transport through early endosomes of polarized Madin-Darby canine kidney cells. Mol. Biol. Cell *17*, 3156–3175.

Balklava, Z., Pant, S., Fares, H., and Grant, B. D. (2007). Genome-wide analysis identifies a general requirement for polarity proteins in endocytic traffic. Nat. Cell Biol *9*, 1066–1073.

Brenner, S. (1974). The genetics of *Caenorhabditis elegans*. Genetics *77*, 71–94.

Brown, P. S., Wang, E., Aroeti, B., Chapin, S. J., Mostov, K. E., and Dunn, K. W. (2000). Definition of distinct compartments in polarized Madin-Darby canine kidney (MDCK) cells for membrane-volume sorting, polarized sorting and apical recycling. Traffic *1*, 124–140.

Burbea, M., Dreier, L., Dittman, J. S., Grunwald, M. E., and Kaplan, J. M. (2002). Ubiquitin and AP180 regulate the abundance of GLR-1 glutamate receptors at postsynaptic elements in *C. elegans*. Neuron *35*, 107–120.

Casanova, J. E., Wang, X., Kumar, R., Bhartur, S. G., Navarre, J., Woodrum, J. E., Altschuler, Y., Ray, G. S., and Goldenring, J. R. (1999). Association of Rab25 and Rab11a with the apical recycling system of polarized Madin-Darby canine kidney cells. Mol. Biol. Cell *10*, 47–61.

Cheeseman, I. M., Niessen, S., Anderson, S., Hyndman, F., Yates, J. R., 3rd, Oegema, K., and Desai, A. (2004). A conserved protein network controls assembly of the outer kinetochore and its ability to sustain tension. Genes Dev. *18*, 2255–2268.

Chen, C. C., Schweinsberg, P. J., Vashist, S., Mareiniss, D. P., Lambie, E. J., and Grant, B. D. (2006). RAB-10 is required for endocytic recycling in the *Caenorhabditis elegans* intestine. Mol. Biol. Cell *17*, 1286–1297.

Chun, D. K., McEwen, J. M., Burbea, M., and Kaplan, J. M. (2008). UNC-108/Rab2 regulates postendocytic trafficking in *Caenorhabditis elegans*. Mol. Biol. Cell *19*, 2682–2695.

Clokey, G. V., and Jacobson, L. A. (1986). The autofluorescent "lipofuscin granules" in the intestinal cells of *Caenorhabditis elegans* are secondary lysosomes. Mech. Ageing Dev. *35*, 79–94.

Daumke, O., Lundmark, R., Vallis, Y., Martens, S., Butler, P. J., and McMahon, H. T. (2007). Architectural and mechanistic insights into an EHD ATPase involved in membrane remodelling. Nature *449*, 923–927.

Fares, H., and Greenwald, I. (2001). Genetic analysis of endocytosis in *Caenorhabditis elegans*: coelomocyte uptake defective mutants. Genetics *159*, 133–145.

Gesbert, F., Sauvonnet, N., and Dautry-Varsat, A. (2004). Clathrin-independent endocytosis and signalling of interleukin 2 receptors IL-2R endocytosis and signalling. Curr. Top. Microbiol. Immunol. *286*, 119–148.

Glodowski, D. R., Chen, C. C., Schaefer, H., Grant, B. D., and Rongo, C. (2007). RAB-10 regulates glutamate receptor recycling in a cholesterol-dependent endocytosis pathway. Mol. Biol. Cell *18*, 4387–4396.

Grant, B., and Hirsh, D. (1999). Receptor-mediated endocytosis in the *Caenorhabditis elegans* oocyte. Mol. Biol. Cell *10*, 4311–4326.

Grant, B. D., and Caplan, S. (2008). Mechanisms of EHD/RME-1 protein function in endocytic transport. Traffic *9*, 2043–2052.

Grant, B. D., and Donaldson, J. G. (2009). Pathways and mechanisms of endocytic recycling. Nat. Rev. Mol. Cell Biol. *10*, 597–608.

Grosshans, B. L., Ortiz, D., and Novick, P. (2006). Rabs and their effectors: achieving specificity in membrane traffic. Proc. Natl. Acad. Sci. USA *103*, 11821–11827.

Guilherme, A., Soriano, N. A., Bose, S., Holik, J., Bose, A., Pomerleau, D. P., Furcinitti, P., Leszyk, J., Corvera, S., and Czech, M. P. (2004a). EHD2 and the novel EH domain binding protein EHBP1 couple endocytosis to the actin cytoskeleton. J. Biol. Chem. *279*, 10593–10605.

Guilherme, A., Soriano, N. A., Furcinitti, P. S., and Czech, M. P. (2004b). Role of EHD1 and EHBP1 in perinuclear sorting and insulin-regulated GLUT4 recycling in 3T3–L1 adipocytes. J. Biol. Chem. *279*, 40062–40075.

Hart, A. C., Sims, S., and Kaplan, J. M. (1995). Synaptic code for sensory modalities revealed by *C. elegans* GLR-1 glutamate receptor. Nature *378*, 82–84.

Hattula, K., Furuhjelm, J., Arffman, A., and Peranen, J. (2002). A Rab8-specific GDP/GTP exchange factor is involved in actin remodeling and polarized membrane transport. Mol. Biol. Cell *13*, 3268–3280.

Hattula, K., Furuhjelm, J., Tikkanen, J., Tanhuanpaa, K., Laakkonen, P., and Peranen, J. (2006). Characterization of the Rab8-specific membrane traffic route linked to protrusion formation. J. Cell Sci. *119*, 4866–4877.

Henry, L., and Sheff, D. R. (2008). Rab8 regulates basolateral secretory, but not recycling, traffic at the recycling endosome. Mol. Biol. Cell *19*, 2059–2068.

Hermann, G. J., Schroeder, L. K., Hieb, C. A., Kershner, A. M., Rabbitts, B. M., Fonarev, P., Grant, B. D., and Priess, J. R. (2005). Genetic analysis of lysosomal trafficking in *Caenorhabditis elegans*. Mol. Biol. Cell *16*, 3273–3288.

Kachur, T. M., Audhya, A., and Pilgrim, D. B. (2008). UNC-45 is required for NMY-2 contractile function in early embryonic polarity establishment and germline cellularization in. C. elegans. Dev. Biol. *314*, 287–299.

Kamath, R. S., and Ahringer, J. (2003). Genome-wide RNAi screening in *Caenorhabditis elegans*. Methods *30*, 313–321.

Knodler, A., Feng, S., Zhang, J., Zhang, X., Das, A., Peranen, J., and Guo, W. (2010). Coordination of Rab8 and Rab11 in primary ciliogenesis. Proc. Natl. Acad. Sci. USA *107*, 6346–6351.

Kouranti, I., Sachse, M., Arouche, N., Goud, B., and Echard, A. (2006). Rab35 regulates an endocytic recycling pathway essential for the terminal steps of cytokinesis. Curr. Biol. *16*, 1719–1725.

Maricq, A. V., Peckol, E., Driscoll, M., and Bargmann, C. I. (1995). Mechanosensory signalling in *C. elegans* mediated by the GLR-1 glutamate receptor. Nature *378*, 78–81.

Maxfield, F. R., and McGraw, T. E. (2004). Endocytic recycling. Nat. Rev. Mol. Cell Biol. *5*, 121–132.

Mellem, J. E., Brockie, P. J., Zheng, Y., Madsen, D. M., and Maricq, A. V. (2002). Decoding of polymodal sensory stimuli by postsynaptic glutamate receptors in *C. elegans*. Neuron *36*, 933–944.

Mukherjee, S., Ghosh, R. N., and Maxfield, F. R. (1997). Endocytosis. Physiol. Rev. *77*, 759–803.

Naslavsky, N., Boehm, M., Backlund, P. S., Jr., and Caplan, S. (2004). Rabenosyn-5 and EHD1 interact and sequentially regulate protein recycling to the plasma membrane. Mol. Biol. Cell *15*, 2410–2422.

Naslavsky, N., Rahajeng, J., Sharma, M., Jovic, M., and Caplan, S. (2006). Interactions between EHD proteins and Rab11-FIP2, a role for EHD3 in early endosomal transport. Mol. Biol. Cell *17*, 163–177.

Nichols, B. (2003). Caveosomes and endocytosis of lipid rafts. J. Cell Sci. *116*, 4707–4714.

Nonet, M. L., Saifee, O., Zhao, H., Rand, J. B., and Wei, L. (1998). Synaptic transmission deficits in *Caenorhabditis elegans* synaptobrevin mutants. J. Neurosci. *18*, 70–80.

Oegema, K., Desai, A., Rybina, S., Kirkham, M., and Hyman, A. A. (2001). Functional analysis of kinetochore assembly in *Caenorhabditis elegans*. J. Cell Biol. *153*, 1209–1226.

Ortiz, D., Medkova, M., Walch-Solimena, C., and Novick, P. (2002). Ypt32 recruits the Sec4p guanine nucleotide exchange factor, Sec2p, to secretory vesicles; evidence for a Rab cascade in yeast. J. Cell Biol. *157*, 1005–1015.

Pant, S., Sharma, M., Patel, K., Caplan, S., Carr, C. M., and Grant, B. D. (2009). AMPH-1/Amphiphysin/Bin1 functions with RME-1/Ehd1 in endocytic recycling. Nat. Cell Biol. *11*, 1399–1410.

Park, E. C., Glodowski, D. R., and Rongo, C. (2009). The ubiquitin ligase RPM-1 and the p38 MAPK PMK-3 regulate AMPA receptor trafficking. PLoS ONE *4*, e4284.

Patton, A., Knuth, S., Schaheen, B., Dang, H., Greenwald, I., and Fares, H. (2005). Endocytosis function of a ligand-gated ion channel homolog in *Caenorhabditis elegans*. Curr. Biol. *15*, 1045–1050.

Pereira-Leal, J. B., and Seabra, M. C. (2001). Evolution of the Rab family of small GTP-binding proteins. J. Mol. Biol. *313*, 889–901.

Powelka, A. M., Sun, J., Li, J., Gao, M., Shaw, L. M., Sonnenberg, A., and Hsu, V. W. (2004). Stimulation-dependent recycling of integrin beta1 regulated by ARF6 and Rab11. Traffic *5*, 20–36.

Praitis, V., Casey, E., Collar, D., and Austin, J. (2001). Creation of low-copy integrated transgenic lines in *Caenorhabditis elegans*. Genetics *157*, 1217–1226.

Radhakrishna, H., and Donaldson, J. G. (1997). ADP-ribosylation factor 6 regulates a novel plasma membrane recycling pathway. J. Cell Biol. *139*, 49–61.

Randhawa, V. K., Ishikura, S., Talior-Volodarsky, I., Cheng, A. W., Patel, N., Hartwig, J. H., and Klip, A. (2008). GLUT4 vesicle recruitment and fusion are differentially regulated by Rac, AS160, and Rab8A in muscle cells. J. Biol. Chem. *283*, 27208–27219.

Rink, J., Ghigo, E., Kalaidzidis, Y., and Zerial, M. (2005). Rab conversion as a mechanism of progression from early to late endosomes. Cell *122*, 735–749.

Rojas, R., Kametaka, S., Haft, C. R., and Bonifacino, J. S. (2007). Interchangeable but essential functions of SNX1 and SNX2 in the association of retromer with endosomes and the trafficking of mannose 6-phosphate receptors. Mol. Cell. Biol. *27*, 1112–1124.

Rongo, C., Whitfield, C. W., Rodal, A., Kim, S. K., and Kaplan, J. M. (1998). LIN-10 is a shared component of the polarized protein localization pathways in neurons and epithelia. Cell *94*, 751–759.

Sano, H., Eguez, L., Teruel, M. N., Fukuda, M., Chuang, T. D., Chavez, J. A., Lienhard, G. E., and McGraw, T. E. (2007). Rab10, a target of the AS160 Rab GAP, is required for insulin-stimulated translocation of GLUT4 to the adipocyte plasma membrane. Cell Metab. *5*, 293–303.

Sato, M., Grant, B. D., Harada, A., and Sato, K. (2008a). Rab11 is required for synchronous secretion of chondroitin proteoglycans after fertilization in *Caenorhabditis elegans*. J. Cell Sci. *121*, 3177–3186.

Sato, M., Sato, K., Fonarev, P., Huang, C. J., Liou, W., and Grant, B. D. (2005). Caenorhabditis elegans RME-6 is a novel regulator of RAB-5 at the clathrin-coated pit. Nat. Cell Biol. *7*, 559–569.

Sato, M., Sato, K., Liou, W., Pant, S., Harada, A., and Grant, B. D. (2008b). Regulation of endocytic recycling by *C. elegans* Rab35 and its regulator RME-4, a coated-pit protein. EMBO J. *27*, 1183–1196.

Sato, T., *et al.* (2007). The Rab8 GTPase regulates apical protein localization in intestinal cells. Nature *448*, 366–369.

Schuck, S., Gerl, M. J., Ang, A., Manninen, A., Keller, P., Mellman, I., and Simons, K. (2007). Rab10 is involved in basolateral transport in polarized Madin-Darby canine kidney cells. Traffic *8*, 47–60.

Sharma, M., Giridharan, S. S., Rahajeng, J., Naslavsky, N., and Caplan, S. (2009). MICAL-L1 links EHD1 to tubular recycling endosomes and regulates receptor recycling. Mol. Biol. Cell *20*, 5181–5194.

Shi, A., Pant, S., Balklava, Z., Chen, C. C., Figueroa, V., and Grant, B. D. (2007). A novel requirement for *C. elegans* Alix/ALX-1 in RME-1-mediated membrane transport. Curr. Biol. *17*, 1913–1924.

Sjoblom, B., Ylanne, J., and Djinovic-Carugo, K. (2008). Novel structural insights into F-actin-binding and novel functions of calponin homology domains. Curr. Opin. Struct. Biol. *18*, 702–708.

Sonnichsen, B., De Renzis, S., Nielsen, E., Rietdorf, J., and Zerial, M. (2000). Distinct membrane domains on endosomes in the recycling pathway visualized by multicolor imaging of Rab4, Rab5, and Rab11. J. Cell Biol. *149*, 901–914.

Stenmark, H. (2009). Rab GTPases as coordinators of vesicle traffic. Nat. Rev. Mol. Cell Biol. *10*, 513–525.

Timmons, L., and Fire, A. (1998). Specific interference by ingested dsRNA. Nature *395*, 854.

van der Sluijs, P., Hull, M., Webster, P., Male, P., Goud, B., and Mellman, I. (1992). The small GTP-binding protein rab4 controls an early sorting event on the endocytic pathway. Cell *70*, 729–740.

Walseng, E., Bakke, O., and Roche, P. A. (2008). Major histocompatibility complex class II-peptide complexes internalize using a clathrin- and dynamin-independent endocytosis pathway. J. Biol. Chem. *283*, 14717–14727.

Weide, T., Teuber, J., Bayer, M., and Barnekow, A. (2003). MICAL-1 isoforms, novel rab1 interacting proteins. Biochem. Biophys. Res. Commun. *306*, 79–86.

Weigert, R., Yeung, A. C., Li, J., and Donaldson, J. G. (2004). Rab22a regulates the recycling of membrane proteins internalized independently of clathrin. Mol. Biol. Cell *15*, 3758–3770.

Yamamura, R., Nishimura, N., Nakatsuji, H., Arase, S., and Sasaki, T. (2008). The interaction of JRAB/MICAL-L2 with Rab8 and Rab13 coordinates the assembly of tight junctions and adherens junctions. Mol. Biol. Cell *19*, 971–983.

Zheng, Y., Brockie, P. J., Mellem, J. E., Madsen, D. M., and Maricq, A. V. (1999). Neuronal control of locomotion in *C. elegans* is modified by a dominant mutation in the GLR-1 ionotropic glutamate receptor. Neuron *24*, 347–361.